

Article

# 2D Newton Schwarz Legendre Collocation Method for a Convection Problem

Darío Martínez <sup>†</sup>, Henar Herrero <sup>†</sup> and Francisco Pla <sup>\*,†</sup>

Department of Mathematics, Faculty of Chemical Sciences and Technologies, University of Castilla-La Mancha, 13071 Ciudad Real, Spain

\* Correspondence: francisco.pla@uclm.es

† These authors contributed equally to this work.

**Abstract:** In this work, an alternate Schwarz domain decomposition method is proposed to solve a Rayleigh–Bénard problem. The problem is modeled with the incompressible Navier–Stokes equations coupled with a heat equation in a rectangular domain. The Boussinesq approximation is considered. The nonlinearity is solved with Newton’s method. Each iteration of Newton’s method is discretized with an alternating Schwarz scheme, and each Schwarz problem is solved with a Legendre collocation method. The original domain is divided into several subdomains in both directions of the plane. Legendre collocation meshes are coarse, so the problem in each subdomain is well conditioned, and the size of the total mesh can grow by increasing the number of subdomains. In this way, the ill conditioning of Legendre collocation is overcome. The present work achieves an efficient alternating Schwarz algorithm such that the number of subdomains can be increased indefinitely in both directions of the plane. The method has been validated with a benchmark with numerical solutions obtained with other methods and with real experiments. Thanks to this domain decomposition method, the aspect ratio and Rayleigh number can be increased considerably by adding subdomains. Rayleigh values near to the turbulent regime can be reached. Namely, the great advantage of this method is that we obtain solutions close to turbulence, or in domains with large aspect ratios, by solving systems of linear equations with well-conditioned matrices of maximum size one thousand. This is an advantage over other methods that require solving systems with huge matrices of the order of several million, usually with conditioning problems. The computational cost is comparable to other methods, and the code is parallelizable.

**Keywords:** turbulence; Rayleigh–Bénard convection; Legendre collocation; domain decomposition method; alternating Schwarz

**PACS:** 47.11.kb; 47.20.Bp

**MSC:** 35Q35; 65N35; 76E06



**Citation:** Martínez, D.; Herrero, H.; Pla, F. 2D Newton Schwarz Legendre Collocation Method for a Convection Problem. *Mathematics* **2022**, *10*, 3718. <https://doi.org/10.3390/math10193718>

Academic Editor: Smirnov Nikolay Nikolaevich

Received: 5 September 2022

Accepted: 7 October 2022

Published: 10 October 2022

**Publisher’s Note:** MDPI stays neutral with regard to jurisdictional claims in published maps and institutional affiliations.



**Copyright:** © 2022 by the authors. Licensee MDPI, Basel, Switzerland. This article is an open access article distributed under the terms and conditions of the Creative Commons Attribution (CC BY) license (<https://creativecommons.org/licenses/by/4.0/>).

## 1. Introduction

Different scales, complex domains, and boundary layers are computational challenges for laminar and turbulent flow models [1–9]. One of these flows is Rayleigh–Bénard convection, in which a layer of fluid is heated from below. The first to systematically study this phenomenon was H. Bénard [10], who observed a pattern of hexagons when heating exceeded a threshold. Lord Rayleigh [11] explained this phenomenon by identifying the destabilizing mechanism as buoyancy. However, this explanation does not correspond to what happens in Bénard’s experiments. Pearson [12] discovered the second destabilizing mechanism, which is changes in surface tension. In this case, the problems are called Bénard–Marangoni. This mechanism is relevant in crystal growth processes [13,14] or ferrofluids in a magnetic field [15]. If the heating is increased further, different states

occur: stationary, periodic, or chaotic states, up to turbulence. Some of these phenomena have been studied in Refs. [16–21], and the monograph [22] provides detailed information about the understanding of this problem. If the mechanism is buoyancy, the problem is called Rayleigh–Bénard, which is the one we address in this work and is also addressed in Refs. [23–27]. The model equations are the incompressible Navier–Stokes equation and the heat equation under the Boussinesq approximation in a bounded domain [28]. Three parameters appear in the model governing the convective motion: the Rayleigh number  $R$  (ratio between the buoyancy and viscous force), the Prandtl number  $Pr$  (ratio between the kinematic viscosity and thermal diffusivity), and the aspect ratio  $\Gamma$  (ratio between the length and the depth of the fluid layer). In geophysical contexts studying the interior of the stars and planets,  $Pr$  is large and the convective flow is dominated by plumes [29,30]. This is the context of this work.

In the case of order one aspect ratio, this problem has been numerically solved with different numerical techniques, mainly finite elements, spectral elements, and collocation methods [26,30]. The collocation methods are high-order methods that allow one to find precise numerical solutions for this problem with coarse meshes [31–34]. The resulting algebraic systems for these methods are ill conditioned when the mesh size [32,34] is increased. The condition number of the matrices resulting from the discretization is large. The maximum size of the mesh is restricted, and it is not possible to obtain solutions with many oscillations that appear in domains with a large aspect ratio or solutions with different scales that arise when the Rayleigh number increases until reaching turbulent states. The same problem can be found in other numerical techniques, i.e., finite differences, finite elements, or spectral elements for fine meshes. The linear systems that appear in the procedure are huge and usually poorly conditioned. One way to avoid this drawback is to use a domain decomposition strategy; examples of this procedure applied to some partial differential equations can be found in Refs. [2,35–40]. The domain is divided into several subdomains, and the problem is numerically solved in each subdomain with a coarse mesh. In this way, ill conditioning is avoided because the numerical method is used on a coarse mesh. Domain decomposition is widely used for fluid dynamics problems. Alternating Schwarz is the most common domain decomposition technique used to solve incompressible Navier–Stokes. The use of this technique for incompressible Navier–Stokes with different numerical methods can be found in Refs. [41–50]. Schwarz domain decomposition methods have been broadly used as a parallelization strategy of fluid flows [4,5,51–53]. The model equations are nonlinear. A way to deal with the nonlinearity is the use of a Newton method. Newton’s method is a powerful nonlinear solver used successfully in many engineering communities. Recent research has introduced improvements and variants on Newton’s method. In Ref. [54], inexact Newton–Krylov and quasi-Newton algorithms for nonlinear elasticity equations are presented. In Ref. [55], a spatial additive Schwarz preconditioned exact Newton method as nonlinear preconditioner for Newton’s method is applied to multiphase flows. In Ref. [56], the advanced Jacobian-Free Newton–Krylov method in a steam generator is studied. Refs. [57,58] modify the Newton increment to ensure global convergence. Newton’s method considered in this work is the standard method that also provides good results for this type of problems (see Refs. [59–63]).

A partial alternating Schwarz method for Navier–Stokes–Boussinesq with aspect ratio one, low Prandtl number, and  $4 \times 4$  subdomains solved with the method of approximate particular solutions can be found in Ref. [64]. In Ref. [30], this problem is solved with a spectral element method for the 3D and the 2D problem for different values of the parameters, showing that the 3D Rayleigh–Bénard problem is quasi two-dimensional for an infinite Prandtl number.

In this work we, achieve an efficient algorithm for the alternating Schwarz method to solve each step of the Newton scheme used to deal with the nonlinearity solved with a Legendre collocation method of a 2D Rayleigh–Bénard problem with infinite Prandtl number [63]. In Ref. [3], the convergence of this methodology was theoretically proven

in an infinite domain when an overlap is considered for a linear approximation to the problem, and some numerical tests were included. The present work achieves an efficient algorithm to solve the fully nonlinear problem with an alternating Schwarz–Newton–Legendre collocation method. The number of subdomains can be indefinitely increased in both directions of the plane. The numerical solutions have been validated by comparing them with solutions obtained with other methods and with physical experiments [29]. Thanks to this domain decomposition, the aspect ratio and the Rayleigh number can be increased considerably by adding domains in any direction. Values of the Rayleigh number for near turbulent regimes can be reached and domains with large aspect ratio can be considered. The great advantage of this method is that we get solutions close to turbulence, or in domains with large aspect ratios, by solving systems of linear equations with well-conditioned matrices of maximum size one thousand. This is the main advantage over other methods that require solving systems with huge matrices of the order of several million, usually badly conditioned that require the use of preconditioners. The method is parallelizable, and, even without parallelizing, the computational cost is affordable.

The article is organized in the following manner. Section 2 provides the mathematical formulation of the Rayleigh–Bénard problem. The numerical method that includes the domain decomposition method is explained in Section 3. The numerical results and a discussion appear in Section 4. Finally, in Section 5, the conclusions are presented.

## 2. Formulation of the Problem

A two-dimensional (2D) fluid layer of depth  $d$  ( $z$  coordinate) lies between two parallel plates of length  $L$  ( $x$  coordinate). The upper plate is at temperature  $T_0$  and the bottom plate is at  $T_1$  such that  $T_1 > T_0$ . A usual way to non-dimensionalize in Rayleigh–Bénard problems is the following:  $x = x'/d, z = z'/d, t = \kappa t'/d^2, \mathbf{u} = d\mathbf{u}'/\kappa, p = d^2 p'/(\rho_0 \kappa \nu)$ , and  $\theta = (\theta' - T_0)/\Delta T$ , where the primes correspond to the quantities with their dimensions,  $x', z'$  space coordinates,  $t'$  time,  $p'$  pressure,  $\mathbf{u}'$  velocity, and  $\theta'$  temperature,  $\kappa$  is the thermal diffusivity,  $\rho_0$  is the mean density,  $\nu$  is the viscosity, and  $\Delta T = T_1 - T_0$ . The Rayleigh and Prandtl numbers are defined as  $R = d^3 \delta g \Delta T / (\nu \kappa)$  and  $Pr = \nu / \kappa$ , where  $g$  is the gravity constant and  $\delta$  is the thermal expansion coefficient. The domain becomes  $\Omega = \{(x, z) \in \mathbb{R} : 0 < x < \Gamma, 0 < z < 1\} = (0, 1) \times (0, \Gamma)$ , where  $\Gamma = L/d$  is the aspect ratio.

The dimensionless forms of the momentum, mass, and energy balance equations that model the problem are [63]:

$$\frac{1}{Pr}(\partial_t \mathbf{u} + \mathbf{u} \cdot \nabla \mathbf{u}) = \Delta \mathbf{u} - \nabla p + R\theta \mathbf{e}_z, \tag{1}$$

$$\nabla \cdot \mathbf{u} = 0, \tag{2}$$

$$\partial_t \theta + \mathbf{u} \cdot \nabla \theta = \Delta \theta, \tag{3}$$

where  $\mathbf{e}_z$  is the upwards vertical unit vector. The boundary conditions come from mantle convection related models [65,66]. They correspond to a rigid bottom wall, and free-slip, non-deformable surfaces at the top and lateral walls, the environment temperature is fixed at the upper plate, and the lateral walls are insulated, and at the bottom, a constant temperature is imposed,

$$\mathbf{u} = \mathbf{0}, \text{ on } z = 0; \partial_z u_x = u_z = 0, \text{ on } z = 1; \partial_x u_z = u_x = 0, \text{ on } x = 0, \Gamma; \tag{4}$$

$$\theta = 0, \text{ on } z = 1; \partial_x \theta = 0, \text{ on } x = 0, \Gamma; \theta = 1, \text{ on } z = 0. \tag{5}$$

The boundary conditions for pressure are obtained using the normal component of the momentum equations on  $x = 0, \Gamma$  and  $z = 1$ , and the continuity equation at  $z = 0$  (see [67,68]). The positivity of the inf-sup constant is guaranteed because these conditions eliminate the parasite modes for pressure [31].

The Prandtl number  $Pr$  is infinite, as usual in mantle convection related problems [63,65,66,69]. We look for stationary solutions, therefore time dependence is not considered, and the problem is:

$$-\Delta \mathbf{u} + \nabla p - R\theta e_z = 0 \text{ in } \Omega, \tag{6}$$

$$\nabla \cdot \mathbf{u} = 0 \text{ in } \Omega, \tag{7}$$

$$-\Delta \theta + \mathbf{u} \cdot \nabla \theta = 0 \text{ in } \Omega, \tag{8}$$

$$\mathcal{B}(\mathbf{u}, \theta, p) = \mathbf{g} \text{ on } \partial\Omega, \tag{9}$$

where  $\mathcal{B}(\mathbf{u}, \theta, p) = \mathbf{g}$  denotes the boundary conditions defined in (4) and (5).

### 3. Numerical Method

Problem (6)–(9) is nonlinear. The nonlinearity is solved with a Newton iteration [67]. Each step of the Newton method is a linear problem in which a Schwarz alternating domain decomposition method is introduced as explained below, and each Schwarz iteration at each subdomain is discretized with a Legendre collocation method [70].

#### 3.1. Newton Iterative for the Nonlinearity

The nonlinearity is solved with an iterative Newton-like method. The iteration  $n$  satisfies  $(\mathbf{u}^n, p^n, \theta^n) = (\mathbf{u}^{n-1} + \tilde{\mathbf{u}}_n, p^{n-1} + \tilde{p}_n, \theta^{n-1} + \tilde{\theta}_n)$ , where  $(\tilde{\mathbf{u}}_n, \tilde{p}_n, \tilde{\theta}_n)$  are the perturbation fields at the  $n$  iteration, and  $(\mathbf{u}^0, p^0, \theta^0)$  is an initial guess approximated solution. Introducing these fields into Equations (6)–(9), the following system of equations for the perturbation fields is obtained (the tildes and the subscripts for the perturbations have been dropped):

$$-\Delta \mathbf{u} + \nabla p - R\theta e_z = \Delta \mathbf{u}^{n-1} - \nabla p^{n-1} + R\theta^{n-1} e_z \text{ in } \Omega, \tag{10}$$

$$\nabla \cdot \mathbf{u} = -\nabla \cdot \mathbf{u}^{n-1} \text{ in } \Omega, \tag{11}$$

$$-\Delta \theta + \mathbf{u} \cdot \nabla \theta^{n-1} + \mathbf{u}^{n-1} \cdot \nabla \theta = \Delta \theta^{n-1} - \mathbf{u}^{n-1} \cdot \nabla \theta^{n-1} \text{ in } \Omega, \tag{12}$$

$$\mathcal{B}(\mathbf{u}, \theta, p) = -\mathcal{B}(\mathbf{u}^{n-1}, \theta^{n-1}, p^{n-1}) + \mathbf{g} \text{ on } \partial\Omega. \tag{13}$$

This is the linear problem to be solved at each step of the Newton method. The numerical solution fields are then  $\mathbf{u}^n = \mathbf{u}^0 + \sum_{i=1}^n \tilde{\mathbf{u}}_i$ ,  $p^n = p^0 + \sum_{i=1}^n \tilde{p}_i$ ,  $\theta^n = \theta^0 + \sum_{i=1}^n \tilde{\theta}_i$ .

#### 3.2. Alternating Schwarz Domain Decomposition

In this section, we introduce an alternating Schwarz domain decomposition method to solve a step of the Newton method (10)–(13). The computational domain  $\Omega$  is split into  $np \times mp$  subdomains of the same size, where  $mp$  is the number of vertical partitions and  $np$  the number of horizontal partitions;  $\Omega$  is a rectangle, and each subdomain is a rectangle of the same size. In Ref. [3], it is proven that two adjacent domains have to share an overlapping area for the algorithm to converge. Partitions marking the position of each subdomain are performed with double points to handle the overlap. A partition with  $2np$  points on the horizontal interval of the domain,  $[0, \Gamma]$ , and another with  $2mp$  points on the vertical interval of the domain,  $[0, 1]$ , are calculated. These partitions are denoted as  $\{\gamma_{-1}^x = 0, \gamma_1^x, \gamma_2^x, \dots, \gamma_{2(np-1)}^x, \gamma_{2np}^x = \Gamma\}$  and  $\{\gamma_{-1}^z = 0, \gamma_1^z, \gamma_2^z, \dots, \gamma_{2(mp-1)}^z, \gamma_{2mp}^z = 1\}$ , respectively. Note that neither  $\gamma_0^x$ , nor  $\gamma_0^z$ , nor  $\gamma_{2np-1}^x$ , nor  $\gamma_{2mp-1}^z$  are considered due to future calculations. These values depend not only on  $mp$  and  $np$ , but also on the Legendre–Gauss–Lobatto (LGL) collocation points. Therefore, they will be calculated in the next section. Then, each subdomain  $\Omega_{q,p}$  is defined as  $\Omega_{q,p} = (\gamma_{2p-3}^x, \gamma_{2p}^x) \times (\gamma_{2q-3}^z, \gamma_{2q}^z)$ ,  $p = 1, \dots, np, q = 1, \dots, mp$ . Each subdomain has length  $\Gamma^x$  and height  $\Gamma^z$ . An example of these partitions is shown in Figure 1 with  $mp = 2$  and  $np = 2$ .

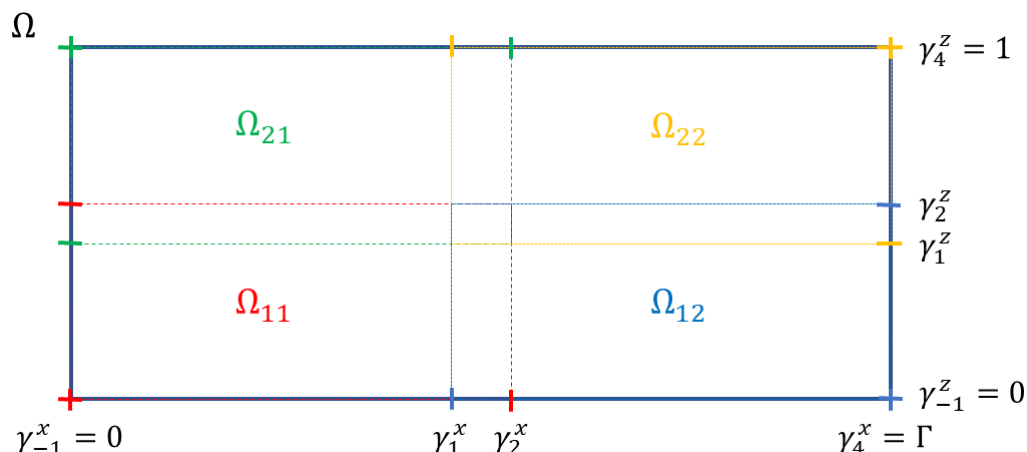


Figure 1. Example of domain  $\Omega$  split in four subdomains with overlap.

Now, the problem has to be adapted to each subdomain  $\Omega_{q,p}$ . The equations inside each subdomain are kept the same. The boundary conditions at the edges of the subdomain, which are also boundaries of the original domain,  $(\partial\Omega_{q,p} \cap \partial\Omega)$ , remain the same. The interfaces are the boundaries of the subdomains, which are inside the original domain  $(\partial\Omega_{q,p} \cap \Omega)$ . The new interface conditions are given by the continuity of the fields  $\mathbf{u}^n$ ,  $p^n$ , and  $\theta^n$ . The previous values in the exact same point of the adjacent rectangle are considered. The following system of equations is solved at each subdomain and each step of the iterative Schwarz method:

$$-\Delta \mathbf{u}_{q,p}^s + \nabla p_{q,p}^s - R\theta_{q,p}^s e_z = -\nabla p_{q,p}^{n-1} + \Delta \mathbf{u}_{q,p}^{n-1} + R\theta_{q,p}^{n-1} e_z \text{ in } \Omega_{q,p}, \tag{14}$$

$$\nabla \cdot \mathbf{u}_{q,p}^s = -\nabla \cdot \mathbf{u}_{q,p}^{n-1} \text{ in } \Omega_{q,p}, \tag{15}$$

$$-\Delta \theta_{q,p}^s + \mathbf{u}_{q,p}^s \cdot \nabla \theta_{q,p}^{n-1} + \mathbf{u}_{q,p}^{n-1} \cdot \nabla \theta_{q,p}^s = \Delta \theta_{q,p}^{n-1} - \mathbf{u}_{q,p}^{n-1} \cdot \nabla \theta_{q,p}^{n-1} \text{ in } \Omega_{q,p}, \tag{16}$$

$$\mathcal{B}(\mathbf{u}_{q,p}^s, \theta_{q,p}^s, p_{q,p}^s) = -\mathcal{B}(\mathbf{u}_{q,p}^{n-1}, \theta_{q,p}^{n-1}, p_{q,p}^{n-1}) + \mathbf{g} \text{ on } \partial\Omega_{q,p} \cap \partial\Omega, \tag{17}$$

$$\mathcal{IB}(\mathbf{u}_{q,p}^s, \theta_{q,p}^s, p_{q,p}^s) = \mathbf{h} \text{ on } \partial\Omega_{q,p} \cap \Omega. \tag{18}$$

The interface boundary conditions  $\mathcal{IB}$  and  $\mathbf{h}$  on  $\partial\Omega_{q,p} \cap \Omega$  are:

$$\mathbf{u}_{q,p}^s = \mathbf{u}_{q',p'}^{s-1} + \mathbf{u}_{q',p'}^{n-1} - \mathbf{u}_{q,p}^{n-1}, \tag{19}$$

$$\theta_{q,p}^s = \theta_{q',p'}^{s-1} + \theta_{q',p'}^{n-1} - \theta_{q,p}^{n-1}, \tag{20}$$

$$p_{q,p}^s = p_{q',p'}^{s-1} + p_{q',p'}^{n-1} - p_{q,p}^{n-1}, \tag{21}$$

where  $q = 1, \dots, mp$ ,  $p = 1, \dots, np$ ,  $(\mathbf{u}_{q,p}^s, p_{q,p}^s, \theta_{q,p}^s)$  are the unknown fields at each subdomain  $\Omega_{q,p}$ ,  $(q', p')$  are the subscripts of the adjacent subdomains, which contain the interface ( $p' = p - 1, p$  or  $p + 1$  and  $q' = q - 1, q$  or  $q + 1$ ),  $s$  denotes the iteration index in the Schwarz algorithm, and  $n$  means the Newton iteration. Note that the continuity of the Newton iterations is considered at the interface, i.e.,  $u_{q,p}^n = u_{q',p'}^n$ , where  $u_{q,p}^n = u_{q,p}^{n-1} + u_{q,p}^s$  and  $u_{q',p'}^n = u_{q',p'}^{n-1} + u_{q',p'}^s$ , and similarly for the rest of the fields. These continuity conditions improve iteration errors.

### 3.3. Legendre Collocation

At each subdomain, the problem is numerically solved with a Legendre collocation method. The Legendre polynomials are defined on the interval  $[-1, 1]$ , therefore, for computational convenience, each subdomain  $\Omega_{q,p}$  is transformed into  $(-1, 1) \times (-1, 1)$

through the following change of variables  $x' = \frac{1}{\Gamma^x}(2x - \gamma_{2p}^x - \gamma_{2p-3}^x)$  and  $z' = \frac{1}{\Gamma^z}(2x - \gamma_{2q}^z - \gamma_{2q-3}^z)$ . These changes of coordinates introduce the corresponding scaling factors in the equations and boundary conditions as follows:  $\partial'_x = \frac{2}{\Gamma^x}\partial_x$  and  $\partial'_z = \frac{2}{\Gamma^z}\partial_z$ . Then, the unknown fields in each subdomain  $\Omega_{q,p}$  are expanded in a truncated series of Legendre polynomials

$$f \simeq f^{NM} = \sum_{l=0}^{N-1} \sum_{k=0}^{M-1} a_{lk}^f L_l(x) L_k(z). \tag{22}$$

The corresponding expansions for the four different fields at the different subdomains are introduced into the equations, the boundary, and the interface conditions, and they are evaluated at the Legendre–Gauss–Lobatto collocation points  $(x_p^l, z_q^k)$  with  $l = 1, 2, \dots, N$  and  $k = 1, 2, \dots, M$ . The Schwarz method requires an *overlap* between adjacent subdomains. The values of  $N$ ,  $M$ , and the number of *overlap* points are known a priori. With all these numbers we can calculate the partitions for the Schwarz method of the interval  $[0, \Gamma]$ ,  $\{\gamma_{-1}^x = 0, \gamma_1^x, \gamma_2^x, \dots, \gamma_{2(np-1)}^x, \gamma_{2np}^x = \Gamma\}$  and the interval  $[0, 1]$ ,  $\{\gamma_{-1}^z = 0, \gamma_1^z, \gamma_2^z, \dots, \gamma_{2(mp-1)}^z, \gamma_{2mp}^z = 1\}$ . Problem (14)–(17) is defined for each subdomain independently. The interface condition requires evaluating the fields at the exact same points in two different subdomains.

The symmetry of the LGL collocation points is very useful for this purpose. If we couple two sets of  $N$  LGL collocation points in such a way that the first point of one of them matches the  $(N - \text{overlap})$ th point of the other, it will occur that the  $(1 + \text{overlap})$ th point of the first set matches the last point of the other set, as shown in Figure 2. This process allows building subdomains with *overlap* shared points. With this information, the partition values can be calculated as follows:  $\gamma_1^x = \frac{\Gamma \cdot x_{N-\text{overlap}}}{(np-1)x_{N-\text{overlap}} + 1}$ ,  $\Gamma^x = \frac{\Gamma}{(np-1)x_{N-\text{overlap}} + 1}$ ,  $\gamma_1^z = \frac{x_{M-\text{overlap}}}{(mp-1)x_{M-\text{overlap}} + 1}$  and  $\Gamma^z = \frac{1}{(mp-1)x_{M-\text{overlap}} + 1}$ , where  $x_p$  is the  $p$ th LGL collocation point. Note that  $\Gamma^x + (np-1)\gamma_1^x = \Gamma$  and  $\Gamma^z + (mp-1)\gamma_1^z = 1$ , as it should be. The other partition values can be calculated recursively knowing these four values, as  $\gamma_{2p-1}^x = p\gamma_1^x$ ,  $\gamma_{2q-1}^z = q\gamma_1^z$ ,  $\gamma_{2(p+1)}^x = \gamma_{2p-1}^x + \Gamma^x$  and  $\gamma_{2(q+1)}^z = \gamma_{2q-1}^z + \Gamma^z$  for  $p = 0, \dots, np-1$  and  $q = 0, \dots, mp-1$ . The solution strategy is mixed with the approximation method.

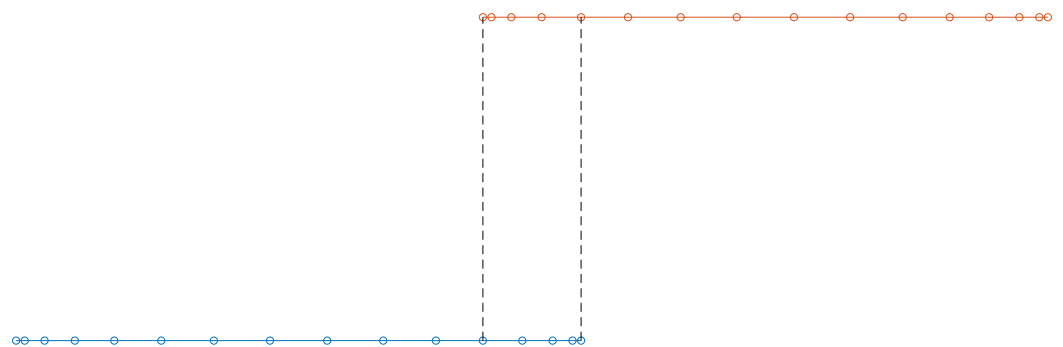


Figure 2. Example of overlap between Legendre collocation nodes in adjacent domains;  $N = 16$ ,  $\text{overlap} = 4$ .

### 3.4. Algorithm

A pseudocode for the algorithm can be summarized as follows:

1. Define input parameters:  $R$ ;  $\Gamma$ ; number of subdomains  $mp \times np$ ; size of the mesh at each subdomain  $N$  ( $x$  direction),  $M$  ( $z$  direction); number of points of overlap,  $o$ ;

2. Introduce fixed parameters in this work: maximum number of Newton iterations,  $stopN = 40$ ; maximum number of Schwarz iterations,  $stopS = 5$ ;
3. Introduce the initial solution in the whole domain:  $u_{x0}, u_{z0}, t_0, p_0$ ;
4. Calculate the part of the solution at each subdomain;
5. Initialize the Newton iteration counter  $Nc = 0$ ;
6. while  $Nc < stopN$  or  $errorN > 10^{-7}$ 
  - (a)  $Nc = Nc + 1$
  - (b) Initialize the Schwarz iteration counter  $Sc = 0$
  - (c) While  $Sc < stopS$  or  $errorS > 10^{-7}$ :
    - i.  $Sc = Sc + 1$ ;
    - ii. For  $q = 1 : mp$  and  $p = 1 : np$  ( $(q, p)$  indicates the subdomain):
      - A. Introduce the corresponding Legendre expansions (22) into equations and boundary conditions (14)–(21), and evaluate at the Legendre–Gauss–Lobatto points, the result is a system of linear algebraic equations;
      - B. Solve the linear system of equations to get the Newton perturbations at each subdomain  $(q, p)$ :  $U_x\{q, p\}, U_z\{q, p\}, T\{q, p\}, P\{q, p\}$ ;
    - iii. End;
    - iv. Calculate the Schwarz errors,  $errorS$ :

$$errorS_{u_x} =$$

$$\begin{aligned} & (||u_x\{1,2\}(:,1+o) + U_x\{1,2\}(:,1+o) - u_x\{1,1\}(:,N) - U_x\{1,1\}(:,N)||_\infty + \\ & ||u_x\{2,1\}(1+o,:) + U_x\{2,1\}(1+o,:) - u_x\{1,1\}(M,:) - U_x\{1,1\}(M,:)||_\infty + \\ & ||u_x\{2,1\}(1,:) + U_x\{2,1\}(1,:) - u_x\{1,1\}(M-o,:) - U_x\{1,1\}(M-o,:)||_\infty + \\ & ||u_x\{1,2\}(:,1) + U_x\{1,2\}(:,1) - u_x\{1,1\}(:,N-o) - U_x\{1,1\}(:,N-o)||_\infty)/4 \end{aligned}$$

$$errorS_{u_z} =$$

$$\begin{aligned} & (||u_z\{1,2\}(:,1+o) + U_z\{1,2\}(:,1+o) - u_z\{1,1\}(:,N) - U_z\{1,1\}(:,N)||_\infty + \\ & ||u_z\{2,1\}(1+o,:) + U_z\{2,1\}(1+o,:) - u_z\{1,1\}(M,:) - U_z\{1,1\}(M,:)||_\infty + \\ & ||u_z\{2,1\}(1,:) + U_z\{2,1\}(1,:) - u_z\{1,1\}(M-o,:) - U_z\{1,1\}(M-o,:)||_\infty + \\ & ||u_z\{1,2\}(:,1) + U_z\{1,2\}(:,1) - u_z\{1,1\}(:,N-o) - U_z\{1,1\}(:,N-o)||_\infty)/4 \end{aligned}$$

$$errorS_\theta =$$

$$\begin{aligned} & (||\theta\{1,2\}(:,1+o) + T\{1,2\}(:,1+o) - \theta\{1,1\}(:,N) - T\{1,1\}(:,N)||_\infty + \\ & ||\theta\{2,1\}(1+o,:) + T\{2,1\}(1+o,:) - \theta\{1,1\}(M,:) - T\{1,1\}(M,:)||_\infty + \\ & ||\theta\{2,1\}(1,:) + T\{2,1\}(1,:) - \theta\{1,1\}(M-o,:) - T\{1,1\}(M-o,:)||_\infty + \\ & ||\theta\{1,2\}(:,1) + T\{1,2\}(:,1) - \theta\{1,1\}(:,N-o) - T\{1,1\}(:,N-o)||_\infty)/4 \end{aligned}$$

$$errorS_p =$$

$$\begin{aligned} & (||p\{1,2\}(:,1+o) + P\{1,2\}(:,1+o) - p\{1,1\}(:,N) - P\{1,1\}(:,N)||_\infty + \\ & ||p\{2,1\}(1+o,:) + P\{2,1\}(1+o,:) - p\{1,1\}(M,:) - P\{1,1\}(M,:)||_\infty + \\ & ||p\{2,1\}(1,:) + P\{2,1\}(1,:) - p\{1,1\}(M-o,:) - P\{1,1\}(M-o,:)||_\infty + \\ & ||p\{1,2\}(:,1) + P\{1,2\}(:,1) - p\{1,1\}(:,N-o) - P\{1,1\}(:,N-o)||_\infty)/4 \end{aligned}$$

$$errorS = errorS_{u_x} + errorS_{u_z} + errorS_\theta + errorS_p$$

- (d) End;

- (e) Update the solution at each subdomain  $(q, p)$ :  $u_{x0}\{q, p\} = u_{x0}\{q, p\} + U_x\{q, p\}$ ;  
 $u_{z0}\{q, p\} = u_{z0}\{q, p\} + U_z\{q, p\}$ ;  $t_0\{q, p\} = t_0\{q, p\} + T\{q, p\}$ ;  $p_0\{q, p\} =$   
 $p_0\{q, p\} + P\{q, p\}$ ;
- (f) Calculate the Newton error:  $Nerror = ||U_x||_\infty + ||U_z||_\infty + ||T||_\infty + ||P||_\infty$  at iteration  $Nc$ .
7. End;
8. Save the results.

#### 4. Numerical Results

Different values of the overlap can be considered with similar results, therefore overlap is fixed to 4 points. Different mesh sizes,  $N$  and  $M$ , between 10 and 18, are considered. Different values of the maximum number of iterations can be taken for the Newton and Schwarz methods. A balance between computational cost and accuracy is obtained by considering a maximum of 40 iterations for Newton's method and a maximum of 5 iterations for Schwarz's method. The iterative initial value for Newton method is a numerical solution calculated with Legendre collocation with expansions  $18 \times 14$  in a domain with aspect ratio  $\Gamma = 3.495$  and  $R = 1300$  adapted to the new multi-domain.

##### 4.1. Validation

Legendre collocation is an ill conditioned method, and the maximum mesh size that can be used in a double precision calculation for parameter values in a laminar regime with a small aspect ratio is  $N \times M = 50 \times 50$ . Some of these values of the parameters are  $R = 1300$  and  $\Gamma = 3.495$ . For this case, we have compared the numerical solutions obtained with Legendre collocation in a single domain with the maximum size of the expansion,  $N \times M = 50 \times 50$ , with numerical solutions obtained with the Newton alternating Schwarz–Legendre collocation method with different numbers of subdomains and different sizes of the Legendre expansions. Table 1 shows the relative  $L^2$  norm of the difference between the horizontal component of the velocity solution,  $u_x$ , obtained with Legendre collocation with a mesh  $50 \times 50$  in a single domain, and the solution obtained with the Newton–Schwarz method with different numbers of subdomains on the horizontal axis,  $np$ , a single domain on the vertical axis,  $mp = 1$ , and different Legendre collocation meshes,  $n$ . The optimal result, taking into account a balance between the coarsest mesh and the smallest error, is obtained with two subdomains on the horizontal axis, one subdomain on the vertical axis, and a Legendre mesh of size  $10 \times 10$ . In this case, the total mesh contains only 200 nodes. Increasing the number of subdomains and/or the size of the mesh at each subdomain makes the solution worse. The same can be seen in Table 2 for two subdomains on the vertical axis, i.e., the relative  $L^2$  norm of the difference between the horizontal component of the velocity solution,  $u_x$ , obtained with Legendre collocation with a mesh  $50 \times 50$  in a single domain, and the solution obtained with the Newton–Schwarz method with different numbers of subdomains on the horizontal axis,  $np$ , two domains on the vertical axis,  $mp = 2$ , and different Legendre collocation meshes  $n$ . Cases with a single domain on the horizontal axis and two subdomains on the vertical do not converge. All other errors are worse than for a single subdomain on the vertical axis. Table 1 shows the optimal result taking into account the size of the total mesh, i.e., two subdomains on the horizontal axis, one subdomain on the vertical axis, and a Legendre mesh of size  $10 \times 10$ .

**Table 1.** Relative  $L^2$  norm of the difference between the horizontal component of the velocity solution,  $u_x$ , obtained with Legendre collocation with a mesh  $50 \times 50$  in a single domain and the solution obtained with different numbers of subdomains on the horizontal axis,  $np$ , a single domain on the vertical axis,  $mp = 1$ , and different Legendre collocation meshes  $N \times M$ ;  $R = 1300$  and  $\Gamma = 3.495$ .

$np$	$10 \times 10$	$14 \times 10$	$16 \times 16$	$28 \times 20$
1	1.2559	0.0324	0.0128	0.0001
2	0.0024	0.0861	0.0749	0.0305
3	0.0351	0.0948	0.1339	0.0525
4	0.0792	0.2341	0.2314	0.1968
5	0.1357	0.2267	0.1846	0.2793
6	0.2054	0.1668	0.1033	0.3871
7	0.2393	0.1274	0.0469	0.4302
8	0.2243	0.0614	0.1568	0.5125
9	0.1809	0.1111	0.2342	0.5476
10	0.1862	0.1882	0.2801	0.6124

**Table 2.** Relative  $L^2$  norm of the difference between the horizontal component of the velocity solution,  $u_x$ , obtained with Legendre collocation with a mesh  $50 \times 50$  in a single domain and the solution obtained with different numbers of subdomains on the horizontal axis,  $np$ , two subdomains on the vertical axis,  $mp = 2$ , and different Legendre collocation meshes  $N \times M$ ;  $R = 1300$  and  $\Gamma = 3.495$ .

$np$	$10 \times 10$	$14 \times 10$	$16 \times 16$	$28 \times 20$
2	0.1165	0.1036	0.0866	0.1591
3	0.1095	0.1493	0.1036	0.1680
4	0.1704	0.1861	0.5280	0.2427
5	0.2013	0.1506	0.0957	0.2887
6	0.1972	0.0939	0.1321	0.3614
7	0.1745	0.0475	0.1818	0.4108
8	0.1387	0.0869	0.2270	0.5032
9	0.1212	0.1530	0.2608	0.5427
10	0.1294	0.2103	0.2868	0.6093

Numerical solutions for larger values of the aspect ratio or larger values of the Rayleigh number cannot be obtained with a single domain, even with the finest mesh. For those cases, the results of the domain decomposition method have been compared with the numerical solutions obtained by means of a finite elements method with a fine mesh with COMSOL. The solutions obtained with both methods can be seen in Figures 3–10 for different values of the parameters. Figure 3 shows solutions obtained with finite elements for  $R = 1300$  and  $\Gamma = 3.495$ . In Figure 4, solutions for the same values of the parameters obtained with alternating Schwarz domain decomposition are presented. This solution has been calculated with two subdomains on the  $x$  axis, one subdomain on the  $z$  axis, and a collocation mesh of size  $N \times M = 10 \times 10$ . Three rolls are observed in both cases. The difference of the maximum value of the temperature field between both solutions is 0.035.

Figure 5 shows solutions obtained with finite elements method for  $R = 1300$  and  $\Gamma = 27.96$ . In Figure 6, solutions for the same values of the parameters obtained with the Schwarz can be seen. This solution has been calculated with 14 subdomains on the horizontal direction, two subdomains on the vertical direction and a collocation mesh of size  $N \times M = 16 \times 10$ . Twenty-five rolls are observed in both solutions. The difference of the maximum value for the temperature field between both solutions is 0.3.

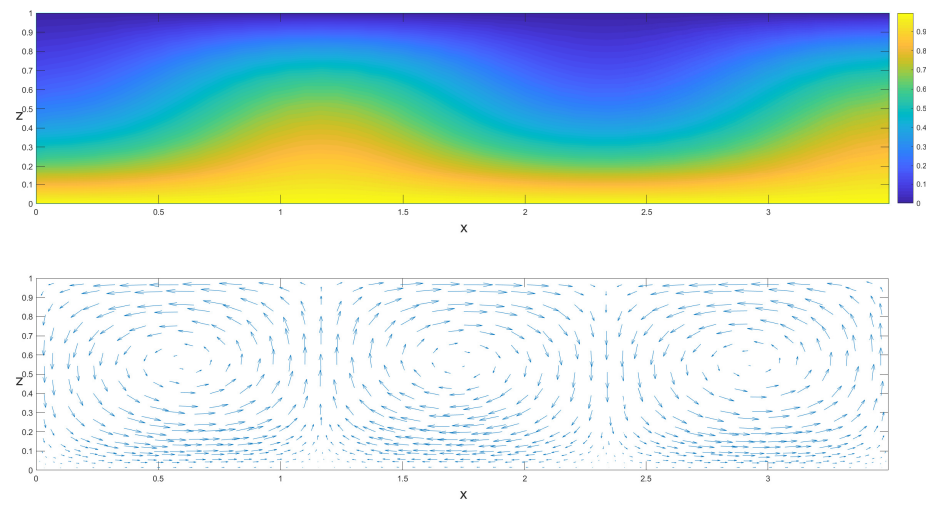


**Figure 3.** Isotherms and velocity field of the numerical solution obtained with finite elements;  $R = 1300$  and  $\Gamma = 3.495$ .

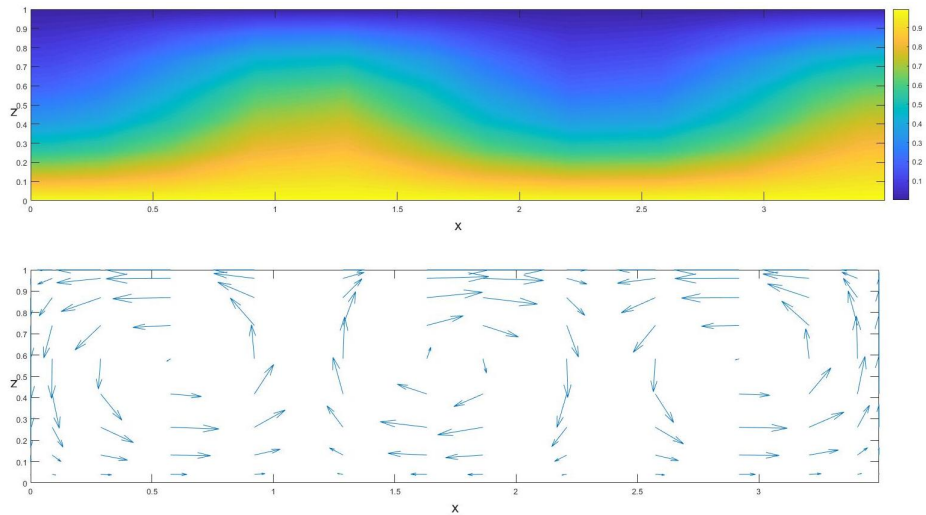


**Figure 4.** Isotherms and velocity field of the numerical solution obtained with alternating Schwarz;  $R = 1300$  and  $\Gamma = 3.495$ .

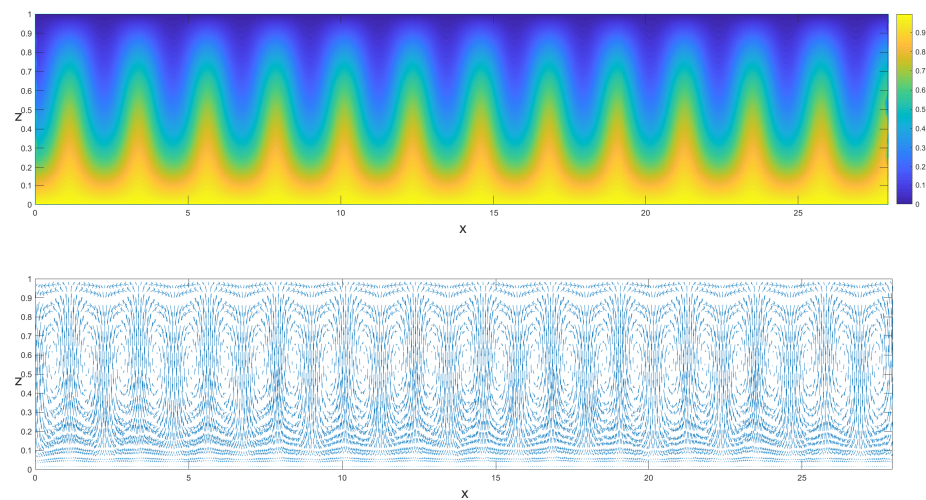


**Figure 5.** Isotherms and velocity field of the numerical solution obtained with finite elements;  $R = 1300$  and  $\Gamma = 27.96$ .

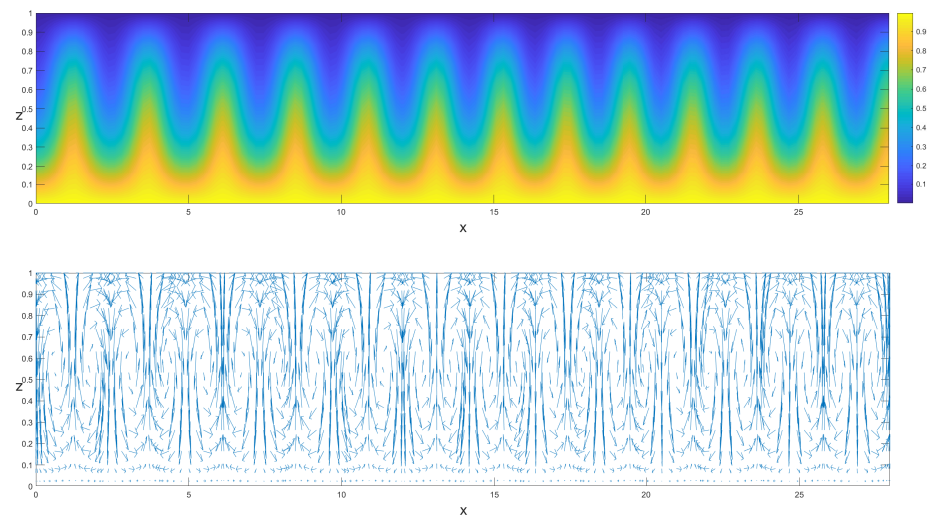


**Figure 6.** Isotherms and velocity field of the numerical solution obtained with alternating Schwarz;  $R = 1300$  and  $\Gamma = 27.96$ .

In Figure 7, solutions obtained with finite elements for  $R = 5000$  and  $\Gamma = 3.495$  are shown. In Figure 8, solutions for the same values of the parameters obtained with the Schwarz method can be seen. This solution has been calculated with eight subdomains on the  $x$  axis, two subdomains on the  $z$  axis, and a collocation mesh of size  $N \times M = 16 \times 10$ . Three rolls are obtained, and the isotherms are mushroom-shaped in both cases. The difference of the maximum value for the temperature field between both solutions is 0.7.

In Figure 9, solutions obtained with finite elements for  $R = 5000$  and  $\Gamma = 27.96$  can be seen. Figure 10 shows solutions for the same values of the parameters obtained with the Schwarz method. This solution has been calculated with 13 subdomains on the  $x$  direction, three subdomains on the  $z$  direction, and a collocation mesh of size  $N \times M = 18 \times 12$ . Twenty-nine rolls are obtained in this case, and the isotherms are mushroom-shaped. The difference of the maximum value for the temperature field between both solutions is 0.6.

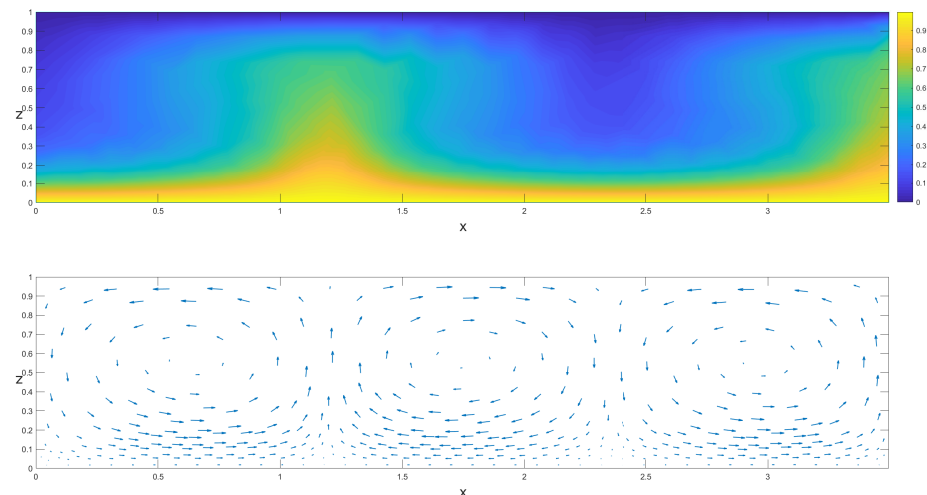


**Figure 7.** Isotherms and velocity field of the numerical solution obtained with finite elements;  $R = 5000$  and  $\Gamma = 3.495$ .

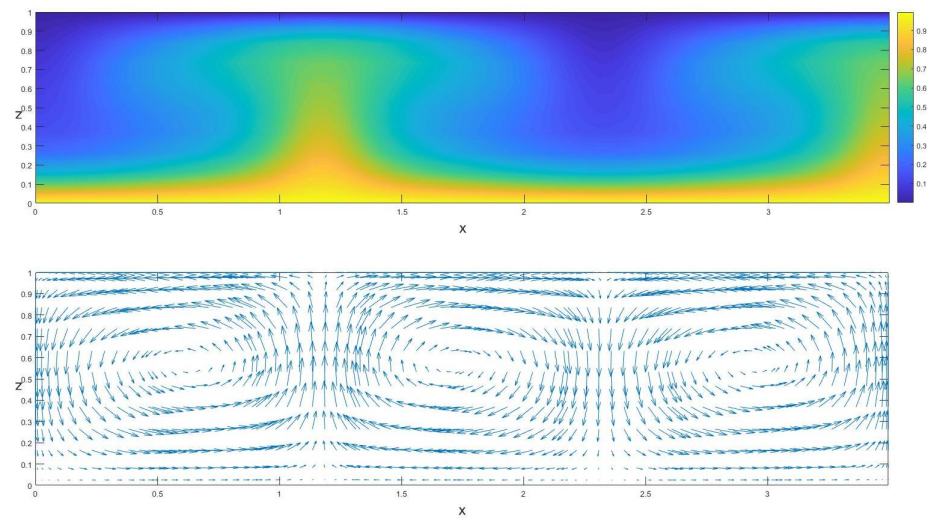


**Figure 8.** Isotherms and velocity field of the numerical solution obtained with alternating Schwarz;  $R = 5000$  and  $\Gamma = 3.495$ .

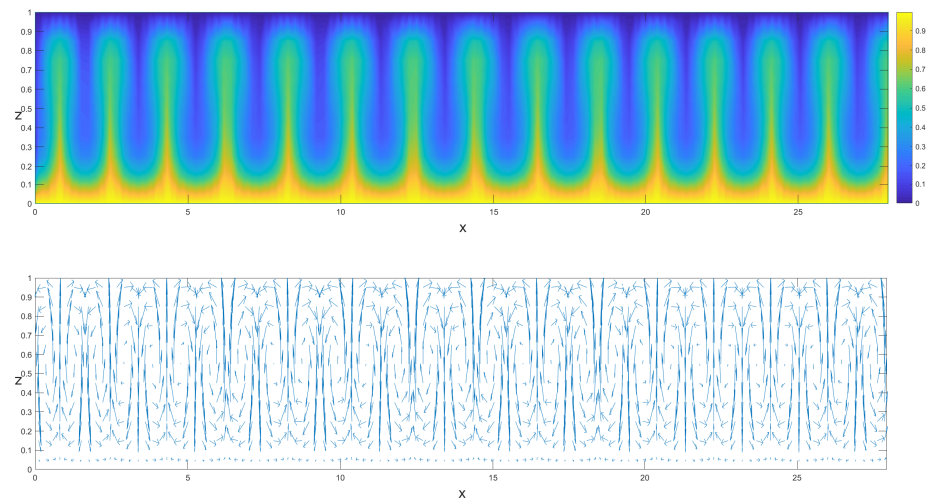


**Figure 9.** Isotherms and velocity field of the numerical solution obtained with finite elements;  $R = 5000$  and  $\Gamma = 27.96$ .

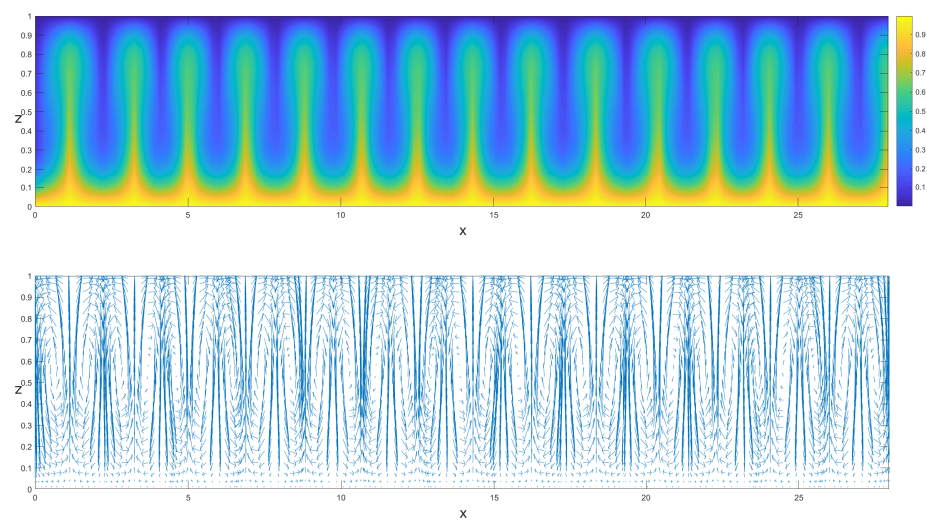


**Figure 10.** Isotherms and velocity field of the numerical solution obtained with alternating Schwarz;  $R = 5000$  and  $\Gamma = 27.96$ .

The same solutions are obtained with the two different numerical methods. There is an optimal value of the number of subdomains that coincides with the minimum number of subdomains.

#### 4.2. Numerical Convergence

The error in the Newton iterations for each field is defined as the Newton perturbations, similarly to the Newton error in Section 3.4, for the first domain:

$$Error_F(n) = \|F^n\|_\infty, \tag{23}$$

where  $F$  refers to any of the fields. The error in the Schwarz iterations for each field is defined similarly to the Schwarz error in Section 3.4 for the first domain and adjacent ones:

$$\begin{aligned} Error_F(s) = & \\ & (\|f^{n-1}\{1,2\}(:,1+4) + F^s\{1,2\}(:,1+4) - f^{n-1}\{1,1\}(:,N) - F^s\{1,1\}(:,N)\|_\infty + \\ & \|f^{n-1}\{2,1\}(1+4,:) + F^s\{2,1\}(1+4,:) - f^{n-1}\{1,1\}(M,:) - F^s\{1,1\}(M,:)\|_\infty + \\ & \|f^{n-1}\{1,2\}(:,1) + F^s\{1,2\}(:,1) - f^{n-1}\{1,1\}(:,N-4) - F^s\{1,1\}(:,N-4)\|_\infty + \\ & \|f^{n-1}\{2,1\}(1,:) + F^s\{2,1\}(1,:) - f^{n-1}\{1,1\}(M-4,:) - F^s\{1,1\}(M-4,:)\|_\infty)/4, \end{aligned}$$

where  $f^{n-1}$  refers to any of the field in the  $(n - 1)$ th Newton iteration,  $F^s$  refers to any of the fields in the  $s$ th Schwarz iteration, and  $4 = overlap$ . Note that  $f^n = f^{n-1} + F^s$  as it has been described in the Newton method, and the Schwarz solution  $F^s$  is the perturbation. Therefore, these errors could be rewritten as

$$\begin{aligned} Error_F(s) = & \\ & (\|f^n\{1,2\}(:,1+4) - f^n\{1,1\}(:,N)\|_\infty + \|f^n\{2,1\}(1+4,:) - f^n\{1,1\}(M,:)\|_\infty + \\ & \|f^n\{1,2\}(:,1) - f^n\{1,1\}(:,N-4)\|_\infty + \|f^n\{2,1\}(1,:) - f^n\{1,1\}(M-4,:)\|_\infty)/4. \end{aligned}$$

We determine the convergence rate of the Schwarz alternating method as the limit of the ratio

$$\frac{Error_F(s+2) - Error_F(s+1)}{Error_F(s+1) - Error_F(s)}. \tag{24}$$

##### 4.2.1. Legendre Collocation

In Tables 3 and 4, we have varied the mesh sizes for two different values of the parameters and a number of subdomains, and we observe that the errors decrease to a minimum and increase as the mesh size increases. The optimum in the case of  $R = 5000$  and  $\Gamma = 3.495$  with eight subdomains on the horizontal axis and  $2 =$  two subdomains on the vertical axis, is  $N = 14$  and  $M = 12$ , which is of the same order as the one used in the figures  $N \times M = 16 \times 10$  with the same number of subdomains. The optimum in the case of  $R = 1300$  and  $\Gamma = 27.96$  with 14 subdomains on the horizontal axis and two subdomains on the vertical axis, is  $N = 14$  and  $M = 10$ , which is of the same order as the one used in the figures  $N \times M = 16 \times 10$  for the same number of subdomains. The optimal mesh size of the expansions is a coarse mesh of order  $10 \times 10$  in each subdomain. Legendre collocation is a high-order method on a single domain, but the global multidomain method with Schwarz and Newton iterations loses this property.

**Table 3.** Newton errors of the last iteration for  $u_x$  obtained with Legendre collocation with different meshes ( $N$  denotes the number of horizontal collocation points and  $M$  denotes the number of vertical collocation points);  $Ra = 5000$ ,  $\Gamma = 3.495$ ,  $np = 8$ , and  $mp = 2$ .

$M \setminus N$	10	12	14	16	18
10	0.0010	0.0017	0.0006	0.0010	0.0019
12	0.0010	0.0006	0.0005	0.0011	0.0022
14	0.0006	0.0006	0.0006	0.0013	0.0027
16	0.0007	0.0006	0.0006	0.0017	0.0034
18	0.0006	0.0006	0.0009	0.0022	0.0044

**Table 4.** Newton errors of the last iteration for  $u_x$  obtained with Legendre collocation with different meshes ( $N$  denotes the number of horizontal collocation points and  $M$  denotes the number of vertical collocation points);  $Ra = 1300$ ,  $\Gamma = 27.96$ ,  $np = 14$ , and  $mp = 2$ .

$M \setminus N$	10	12	14	16	18
10	0.0119	0.0097	0.0101	0.0124	0.0202
12	0.1071	0.0780	0.0638	0.0914	0.0761
14	0.0886	0.0830	0.0781	0.0903	0.0748
16	0.0766	0.0523	0.0540	0.0531	0.0509
18	0.0642	0.0398	0.0341	0.0366	0.0376

#### 4.2.2. Schwarz

In this section, we analyze the behavior of the Schwarz parts of the algorithm, the errors, convergence rate, number of subdomains, and influence of the parameters.

First, we look at the minimum number of subdomains necessary to obtain convergence depending on the parameters present in the problem. Two examples are shown in Tables 5 and 6. In Table 6, the last error in the Newton iteration for the field  $u_x$ , for  $R = 1300$  and  $\Gamma = 27.96$ , increases in the number of subdomains in the vertical and horizontal directions can be seen. A minimum number of subdomains is required to achieve convergence. The minimum number of subdomains to get convergence is  $mp = 2$  and  $np = 3$ , or  $mp = 3$  and  $np = 3$ . A single domain in the vertical direction or one or two subdomains in the horizontal direction never converges. In the case of  $R = 5000$  and  $\Gamma = 3,495$ , in Table 5, the minimum number of subdomains corresponds to  $mp = 1$  and  $np = 8$ , or  $mp = 2$  and  $np = 6$ , or  $mp = 3$  and  $np = 2$ . The number of Schwarz subdomains required increases with  $R$  and  $\Gamma$ , i.e., one domain is enough for  $R = 10^3$ , and around one hundred subdomains are required for  $R = 10^5$  or  $\Gamma = 100$  with the same size of the mesh at each subdomain.

**Table 5.** Newton errors of the last iteration for  $u_x$  obtained with Legendre collocation with a mesh  $16 \times 10$  varying the number of horizontal ( $np$ ) and vertical ( $mp$ ) subdomains;  $Ra = 5000$  and  $\Gamma = 3.495$ .

$np \setminus mp$	1	2	3
1	-	-	-
2	-	-	0.0006
3	-	-	0.0003
4	-	-	0.0002
5	-	-	0.0010
6	-	0.0028	0.0007
7	-	0.0007	0.0009
8	0.0008	0.0010	0.0014
9	0.0018	0.0020	0.0030
10	0.0063	0.0063	0.0074

**Table 6.** Newton errors of the last iteration for  $u_x$  obtained with Legendre collocation with a mesh  $16 \times 10$  varying the number of horizontal ( $np$ ) and vertical ( $mp$ ) subdomains;  $Ra = 1300$  and  $\Gamma = 27.96$ .

$np \backslash mp$	1	2	3
1	-	-	-
2	-	-	-
3	-	0.0104	0.0632
4	-	0.0573	0.0694
5	-	0.0283	0.1036
6	-	0.0770	0.0702
7	-	0.0069	0.0730
8	-	0.0130	0.0778
9	-	0.0253	0.0753
10	-	0.0044	0.0727
11	-	0.0101	0.0777
12	-	0.0209	0.0708
13	-	0.0417	0.0605
14	-	0.0124	0.0981
15	-	0.0327	0.0994
16	-	0.0638	0.0971

Second, we study the influence of the parameters in the Schwarz errors. First, we vary the Rayleigh number. In Figure 11a, the decimal logarithm of the errors in the velocity, temperature, and pressure fields for the Schwarz iterations in the case  $R = 1300$ ,  $\Gamma = 3.495$ ,  $np = 2$ ,  $mp = 1$ , and  $N \times M = 10 \times 10$ , can be seen. In that figure, we can check the convergence of Schwarz’s method for each Newton problem. The errors of the Schwarz solver reach values between  $10^{-8}$  and  $10^{-9}$  for all fields as Newton’s problems progress. Figure 11b shows the decimal logarithm of the errors in the four fields for the Schwarz iterations in the case  $R = 5000$ ,  $\Gamma = 3.495$ ,  $np = 8$ ,  $mp = 2$ , and  $N \times M = 16 \times 10$ . The errors for the Schwarz iterations reach values between  $10^{-5}$  and  $10^{-6}$  for all the fields. In that figure, the convergence of Schwarz for each Newton problem can be seen. We have increased further the Rayleigh number for a fixed value of the aspect ratio,  $\Gamma = 3.495$ . Figure 12 shows a solution for  $R = 10^4$  obtained with 25 subdomains on the horizontal axis and two subdomains on the vertical axis for a collocation mesh of  $12 \times 10$ . The three rolls with the mushroom shaped isotherms still remain. In Figure 13, a solution for  $R = 10^5$  obtained with 25 subdomains on the horizontal axis and five subdomains on the vertical axis for a collocation mesh of  $16 \times 12$  can be seen. Eleven rolls with plume shaped isotherms is a new solution in the near turbulent regime. Figure 14a, shows the decimal logarithm of the errors in the velocity, temperature, and pressure fields for the Schwarz iterations in the case of  $R = 10^4$  and  $\Gamma = 3.495$ . These errors take values between  $10^{-4}$  and  $10^{-3}$ . Figure 14b shows the decimal logarithm of the errors in the velocity, temperature, and pressure fields for the Schwarz iterations in the case of  $R = 10^5$  and  $\Gamma = 3.495$ . In that figure, the convergence of Schwarz for each Newton problem is tested. The errors for the Schwarz solver reach values between  $10^{-5}$  and  $10^{-4}$ . The increase in  $R$  needs an increase in the number of subdomains to reach convergence. There is a loss of accuracy of the method with  $R$  or with the increase in the number of subdomains.

Now we increase the values of the aspect ratio and the Rayleigh number. The decimal logarithm of the errors in the velocity, temperature, and pressure fields for the Schwarz iterations in the case of  $R = 1300$ ,  $\Gamma = 27.96$ ,  $np = 14$ ,  $mp = 2$ , and  $N \times M = 16 \times 10$ , can be seen in Figure 15a. The convergence of the Schwarz method for each Newton problem is shown in this figure. The errors for the Schwarz solver reach values between  $10^{-5}$  and  $10^{-4}$  for all the fields. Figure 15b shows the decimal logarithm of the errors in the four fields for the Schwarz iterations in the case of  $R = 5000$ ,  $\Gamma = 27.96$ ,  $np = 13$ ,  $mp = 3$ , and  $N \times M = 18 \times 12$ . These errors take values between  $10^{-4}$  and  $10^{-3}$ . If we compare with the previous results in the case of  $\Gamma = 3.495$ , the increase in  $\Gamma$  needs an increase in the number

of subdomains to reach convergence. There is a loss of accuracy of the method with  $\Gamma$  or with the increase in the number of subdomains.

We have increased further the aspect ratio for a fixed value of the Rayleigh number,  $R = 1300$ . Figure 16 shows a solution for  $\Gamma = 50$  obtained with 20 subdomains on the horizontal axis and two subdomains on the vertical axis for a collocation mesh of  $16 \times 10$ . The number of rolls increases. Figure 17 shows a solution for  $\Gamma = 100$  obtained with 35 subdomains on the horizontal axis and two subdomains on the vertical axis for a collocation mesh of  $16 \times 10$ . The number of rolls doubles. The number of necessary subdomains increases with  $\Gamma$  in a nearly logarithmic way. A noteworthy aspect is that the values of the aspect ratio can be increased as much as required.

The convergence rate for the Schwarz iterations appears in Figure 18a,b. The convergence rate are 0.7 in the first case and 0.9 in the second case. There is a dependence of the convergence rate with the parameters; it increases with  $R$  and  $\Gamma$ , although it always remains less than 1.

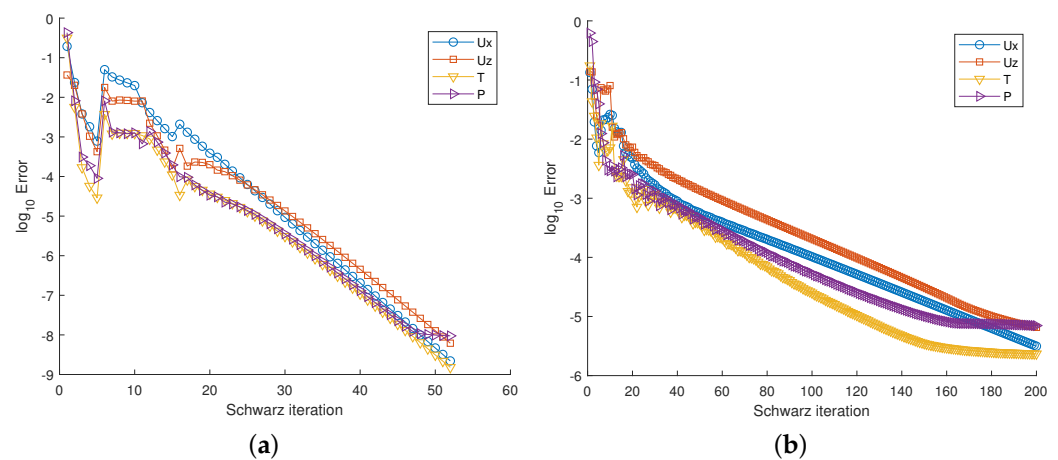


**Figure 11.** Graph of the  $\log_{10}$  of the errors in the velocity, temperature, and pressure fields for the Schwarz iterations: (a)  $R = 1300$ ,  $\Gamma = 3.495$ ,  $np = 2$ ,  $mp = 1$ ,  $N \times M = 10 \times 10$ ; (b)  $R = 5000$ ,  $\Gamma = 3.495$ ,  $np = 8$ ,  $mp = 2$ ,  $N \times M = 16 \times 10$ .

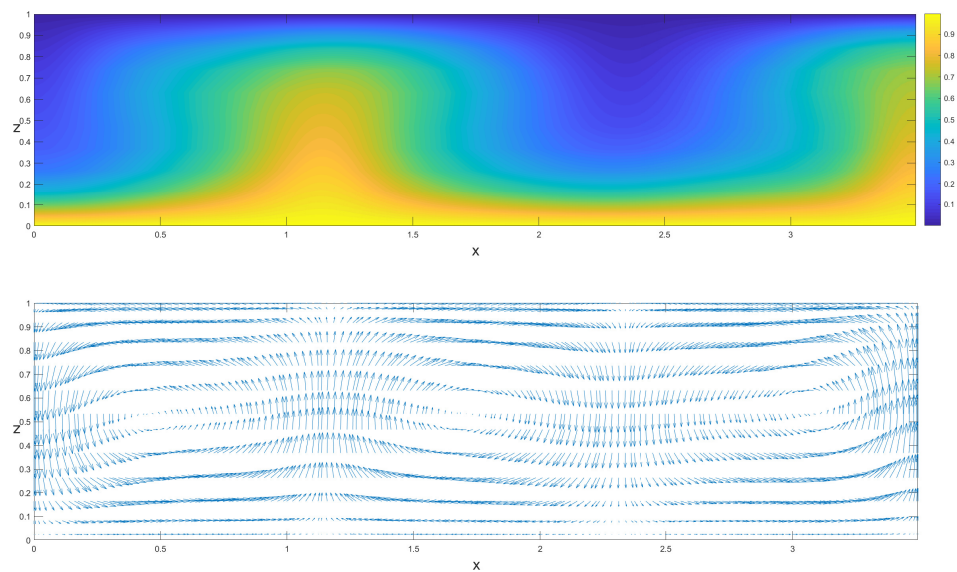


**Figure 12.** Isotherms and velocity field of a numerical solution obtained with alternating Schwarz domain decomposition;  $R = 10^4$ ,  $\Gamma = 3.495$ ,  $np = 25$ ,  $mp = 2$ ,  $N \times M = 12 \times 10$ .

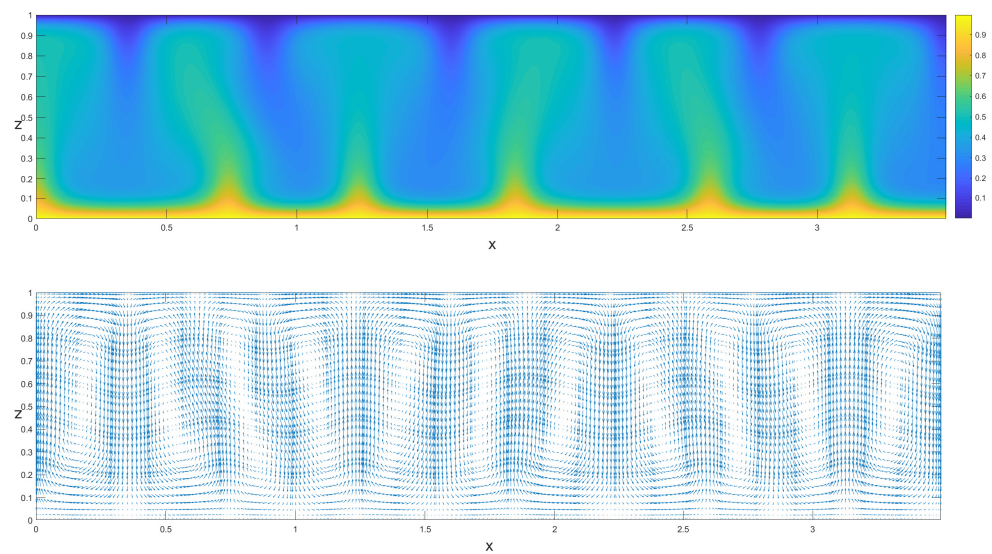


**Figure 13.** Isotherms and velocity field of a numerical solution obtained with alternating Schwarz domain decomposition;  $R = 10^5$ ,  $\Gamma = 3.495$ ,  $np = 25$ ,  $mp = 5$ ,  $N \times M = 16 \times 12$ .

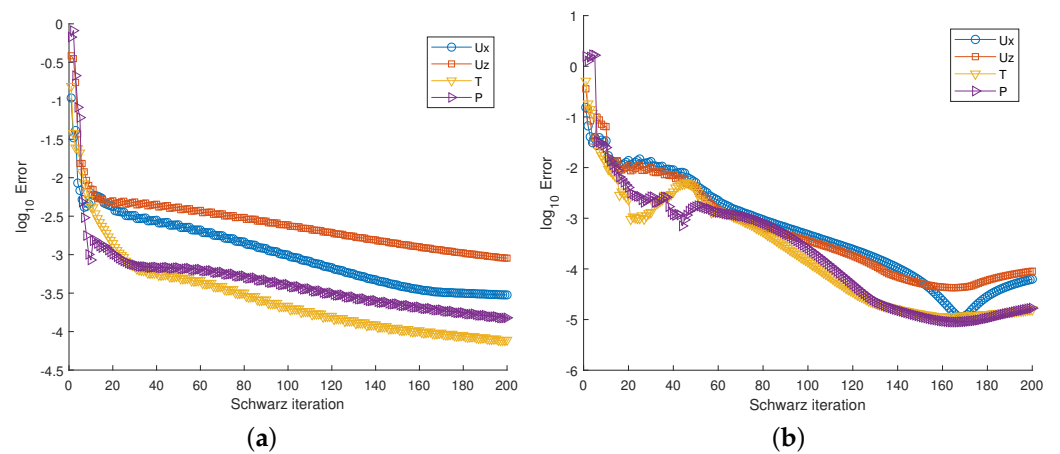


**Figure 14.** Graph of the  $\log_{10}$  of the errors in the velocity, temperature, and pressure fields for the Schwarz iterations: (a)  $R = 10^4$ ,  $\Gamma = 3.495$ ,  $np = 25$ ,  $mp = 2$ ,  $N \times M = 12 \times 10$ ; (b)  $R = 10^5$ ,  $\Gamma = 3.495$ ,  $np = 25$ ,  $mp = 5$ ,  $N \times M = 16 \times 12$ .

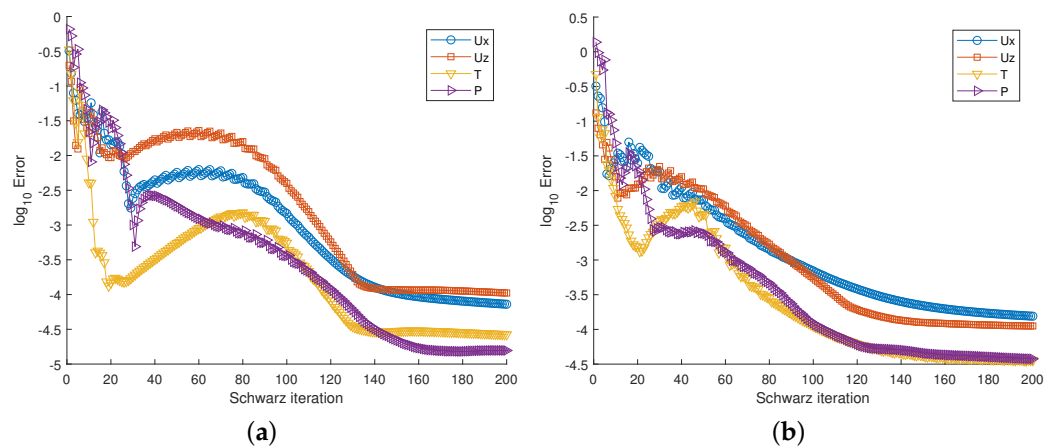


**Figure 15.** Graph of the  $\log_{10}$  of the errors in the velocity, temperature, and pressure fields for the Schwarz iterations: (a)  $R = 1300$ ,  $\Gamma = 27.96$ ,  $np = 14$ ,  $mp = 2$ ,  $N \times M = 16 \times 10$ ; (b)  $R = 5000$ ,  $\Gamma = 27.96$ ,  $np = 13$ ,  $mp = 3$ ,  $N \times M = 18 \times 12$ .

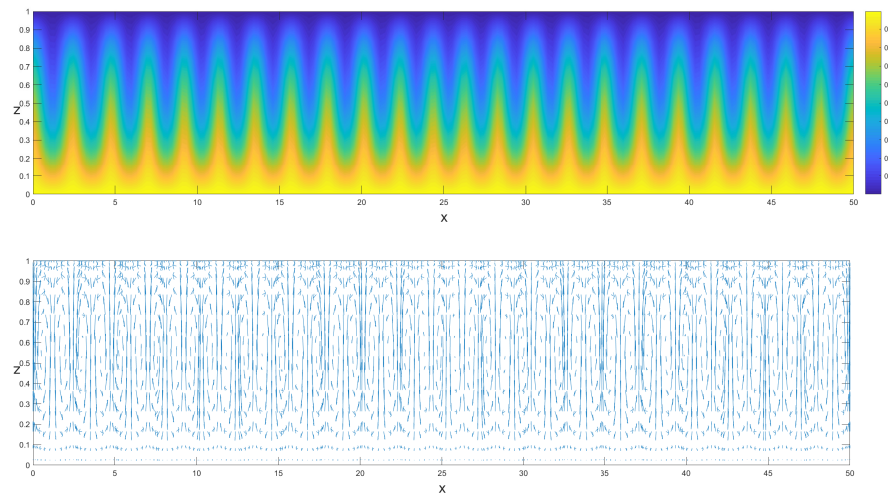


**Figure 16.** Isotherms and velocity field of a numerical solution obtained with alternating Schwarz domain decomposition;  $R = 1300, \Gamma = 50, np = 20, mp = 2, N \times M = 16 \times 10$ .

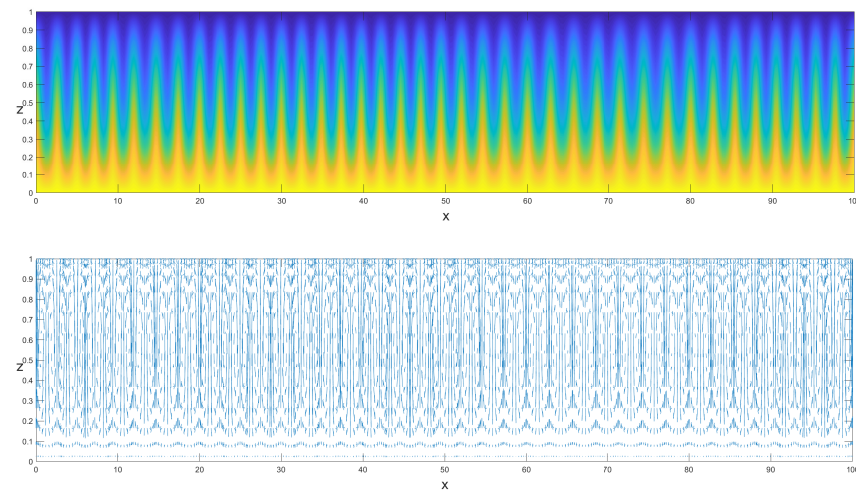


**Figure 17.** Isotherms and velocity field of a numerical solution obtained with alternating Schwarz domain decomposition;  $R = 1300, \Gamma = 100, np = 35, mp = 2, N \times M = 16 \times 10$ .

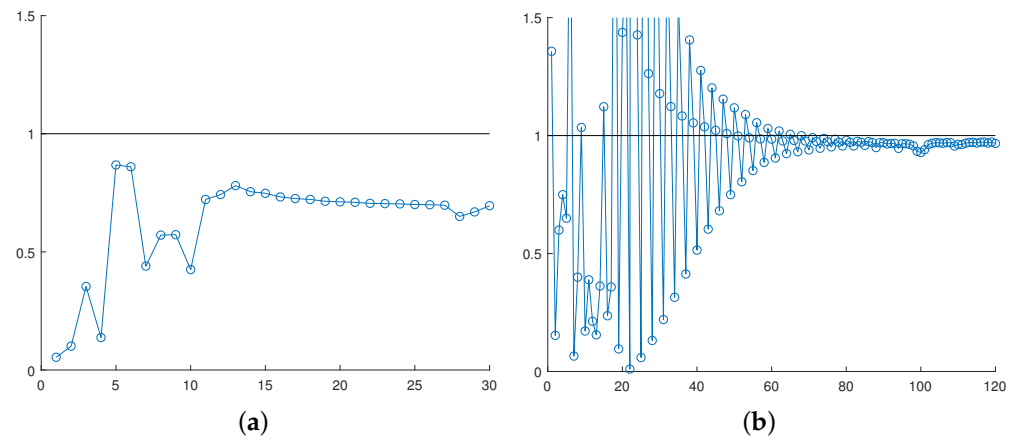


**Figure 18.** (a) Convergence rate for the Schwarz iterations:  $R = 1300, \Gamma = 3.495$ ; (b) convergence rate for the Schwarz iterations:  $R = 5000, \Gamma = 3.495$ .

### 4.2.3. Newton

In this section, we analyze the behavior of the Newton method, the errors, convergence rate, number of subdomains, and influence of the parameters.

First, we investigate the influence of the Rayleigh number for a fixed value of the aspect ratio  $\Gamma = 3.495$ . Figure 19a shows the decimal logarithm of the errors in the velocity, temperature, and pressure fields for the Newton iterations for  $R = 1300$ ,  $\Gamma = 3.495$ ,  $np = 2$ , and  $mp = 1$ . Newton’s errors are  $10^{-8}$  for the temperature field and  $10^{-7}$  for both components of the velocity field and the pressure field. This figure shows the convergence of the nonlinear method. Figure 19b shows the decimal logarithm of the errors in the four fields for the Newton iterations for  $R = 5000$ ,  $\Gamma = 3.495$ ,  $np = 8$ , and  $mp = 2$ . The Newton errors are around  $10^{-3}$  for all the fields. Figure 20a shows the decimal logarithm of the errors for the Newton iterations for  $R = 10^4$  and  $\Gamma = 3.495$ . These errors are between  $10^{-2}$  and  $10^{-1}$ . The convergence of the nonlinear problem is shown in this figure. Figure 20b shows the decimal logarithm of the errors for the Newton iterations for  $R = 10^5$  and  $\Gamma = 3.495$ . The Newton errors are between  $10^{-2}$  and  $10^{-1}$ . The method is convergent. The increase in  $R$  needs an increase in the number of subdomains to reach convergence. There is a loss of accuracy of the method with  $R$  or with the increase in the number of subdomains.

Now we increase the Rayleigh number and the aspect ratio. The decimal logarithm of the errors in the velocity, temperature, and pressure fields for the Newton iterations for  $R = 1300$ ,  $\Gamma = 27.96$ ,  $np = 14$ , and  $mp = 2$  are shown in Figure 21a. The Newton errors are around  $10^{-2}$ . Convergence of the nonlinear problem is shown in this figure. In Figure 21b, the decimal logarithm of the errors in the fields for the Newton iterations for  $R = 5000$ ,  $\Gamma = 27.95$ ,  $np = 13$ , and  $mp = 3$  can be seen. These errors are around  $10^{-2}$ . The method is convergent. If we compare with the previous results in the case of  $\Gamma = 3.495$ , the increase in  $\Gamma$  needs an increase in the number of subdomains to reach convergence. There is a loss of accuracy of the method with  $\Gamma$  or with the increase in the number of subdomains.

Newton’s method has a second-order local rate of convergence in the single-domain case. This has been shown in the case of the Legendre collocation in a single domain in Figure 22, where the numerical sequence  $\frac{|u_x^{n+2} - u_x^{n+1}|}{|u_x^{n+1} - u_x^n|^2}$ ,  $n = 1, 2, \dots$  for  $R = 1300$ ,  $\Gamma = 3.495$ ,  $np = 1$ ,  $mp = 1$ ,  $N \times M = 50 \times 50$ , has been plotted, and the tendency to 1 can be seen. For a single domain, the iterations are just Newton iterations. However, in the multi-domain case, Schwarz iterations are introduced at each Newton iteration, and the errors due to those iterations become relevant. In the multi-domain case with Schwarz iterations, Newton’s method becomes first order, as can be seen in Figure 23, where the numerical sequence  $\frac{|u_x^{n+2} - u_x^{n+1}|}{|u_x^{n+1} - u_x^n|}$ ,  $n = 1, 2, \dots$  for the same case and two horizontal subdomains has been plotted, the tendency to 0.17 can be seen.

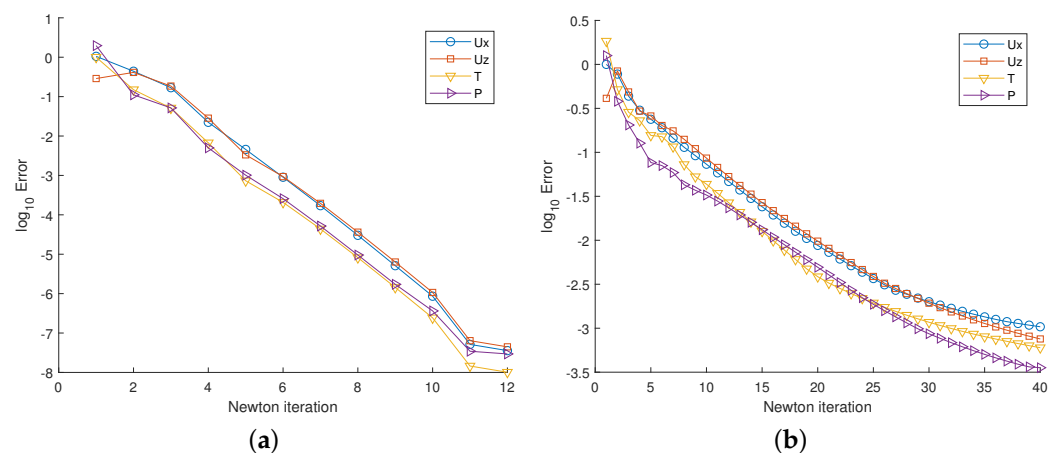


**Figure 19.** Graph of the  $\log_{10}$  of the errors in the velocity, temperature, and pressure fields for the Newton iterations: (a)  $R = 1300$ ,  $\Gamma = 3.495$ ,  $np = 2$ ,  $mp = 1$ ,  $N \times M = 10 \times 10$ ; (b)  $R = 5000$ ,  $\Gamma = 3.495$ ,  $np = 8$ ,  $mp = 2$ ,  $N \times M = 16 \times 10$ .

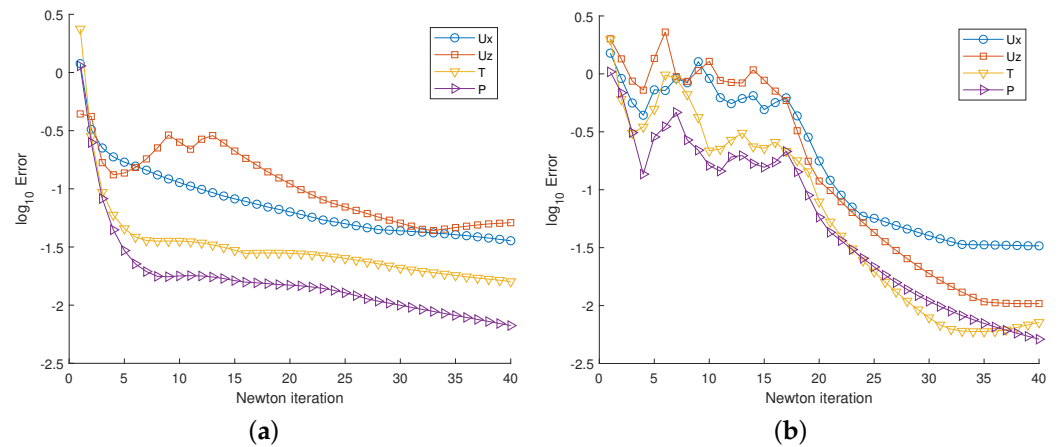


**Figure 20.** Graph of the  $\log_{10}$  of the errors in the velocity, temperature, and pressure fields for the Newton iterations: **(a)**  $R = 10^4$ ,  $\Gamma = 3.495$ ,  $np = 25$ ,  $mp = 2$ ,  $N \times M = 12 \times 10$ ; **(b)**  $R = 10^5$ ,  $\Gamma = 3.495$ ,  $np = 25$ ,  $mp = 5$ ,  $N \times M = 16 \times 12$ .

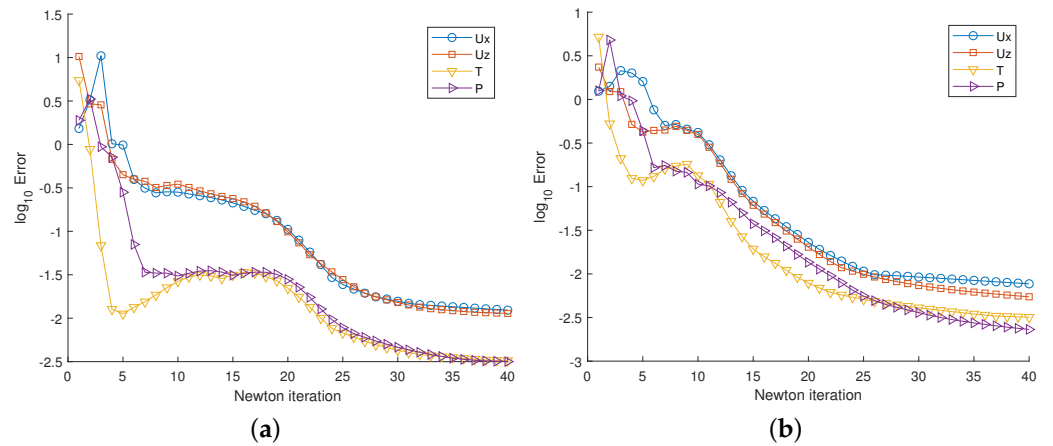


**Figure 21.** Graph of the  $\log_{10}$  of the errors in the velocity, temperature, and pressure fields for the Newton iterations: **(a)**  $R = 1300$ ,  $\Gamma = 27.96$ ,  $np = 14$ ,  $mp = 2$ ,  $N \times M = 16 \times 10$ ; **(b)**  $R = 5000$ ,  $\Gamma = 27.96$ ,  $np = 13$ ,  $mp = 3$ ,  $N \times M = 18 \times 12$ .

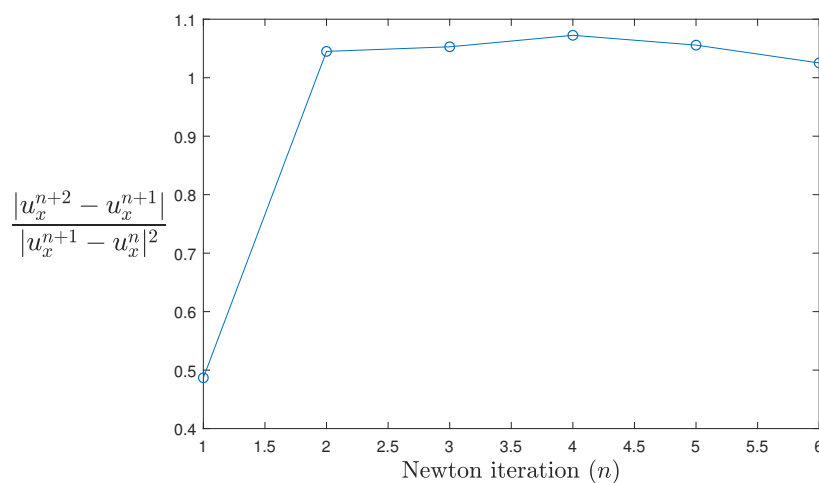


**Figure 22.** Ratio of the convergence of the Newton's method for  $R = 1300$ ,  $\Gamma = 3.495$ ,  $np = 1$ ,  $mp = 1$ ,  $N \times M = 50 \times 50$ .

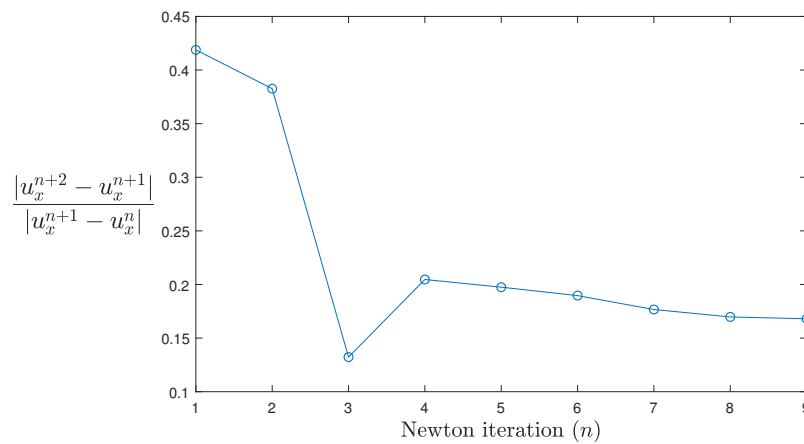


**Figure 23.** Ratio of the convergence of the Newton’s method for  $R = 1300$ ,  $\Gamma = 3.495$ ,  $np = 2$ ,  $mp = 1$ ,  $N \times M = 16 \times 10$ .

### 4.3. Computational Cost

Next, we study the computational cost. We approximate the number of operations considering only products. We name  $n = N \times M$ ,  $N_t = 4n$ ,  $N_S$ : number of iterations of the Schwarz solver,  $N_N$ : number of iterations of the Newton procedure. Each Newton and Schwarz iteration solves a linear system of size  $N_t$  with a computational cost  $O(N_t^2)$ ; then, to calculate the total computational cost, we multiply by the number of subdomains and the number of Newton and Schwarz iterations, then the total number of operations is  $No = np \cdot mp \cdot N_S \cdot N_N \cdot N_t^2$ . In the smallest case considered in this work,  $R = 1300$ ,  $\Gamma = 3.495$ ,  $N_t = 4 \times 10 \times 10$ ,  $N_S = 5$ ,  $N_N = 12$ ,  $np = 2$ ,  $mp = 1$ ,  $No = 2 \times 10^7$ . In the case of large aspect ratio,  $\Gamma = 50$ ,  $np = 25$ ,  $mp = 2$ ,  $N_S = 5$ ,  $N_N = 40$ , then  $No = 4 \times 10^9$ . In the case of large aspect ratio,  $\Gamma = 100$ ,  $np = 50$ ,  $mp = 2$ ,  $N_S = 5$ ,  $N_N = 40$ , then  $No = 6 \times 10^9$ . The case of large Rayleigh number  $R = 10^5$ ,  $np = 25$ ,  $mp = 5$ ,  $N_S = 5$ ,  $N_N = 40$ , then  $No = 10^{10}$ . In a parallel computation, if we do not take into account the computational cost penalty due to parallelization, the calculation would run at the same time in each subdomain, then the number of subdomains would be saved, and the number of operations would be reduced to  $Nop = N_S \cdot N_N \cdot N_t^2$ .

Regarding computing time, the calculations have been performed with a 4 GHz Intel Core i7 microprocessor. For instance, in the case of  $R = 1300$ ,  $\Gamma = 100$ , with 50 subdomains on the  $x$  axis and two subdomains on the  $z$  axis, with a Legendre mesh of  $N_t = 4 \times 16 \times 10$ , the computing time is 612 s. This time could be reduced the order of magnitude associated with the total number of subdomains in an ideal parallel computation. The order of reduction is  $np \cdot mp$ , and the time computing is  $N_S \times N_N$  the time it takes to solve a linear system of size  $N_t$ .

### 4.4. Discussion

This method includes several elements, validation, Legendre collocation method, Schwarz iterations, Newton iterations, turbulence, and computational cost.

From the point of view of validation, the equations have been solved with finite elements and with the present method. The same solutions are obtained with both methods. The same states of rolls and thermal plumes are observed in the real physical experiments [29].

We look now at the Legendre collocation method. The optimal mesh size of the expansions is a coarse mesh of order  $10 \times 10$  in each subdomain. Legendre collocation is a high-order method in a single domain, but the global multi-domain method with the Schwarz and Newton iterations loses this property.

With respect to the Schwarz method, the Schwarz parts of the method converge, the errors are on the order of  $10^{-4}$  or less, and the convergence rate is less than 1 for all the fields and values of the parameters present in the problem. There is a dependence of the

convergence rate with the parameters; it increases with  $R$  and  $\Gamma$ , although it always remains less than 1. The minimum distribution of necessary subdomains to reach convergence depends on  $R$  and  $\Gamma$ ; it increases with both parameters with a logarithmic dependence.

In relation with the Newton method, it converges, and the final errors increase with the parameters  $R$  and  $\Gamma$ , varying from  $10^{-8}$  for the lower values  $R = 1300$  and  $\Gamma = 3.495$ , to  $10^{-2}$  for the larger values  $R = 5000$  and  $\Gamma = 3.495$ . Newton's method has a second-order local rate of convergence in the single-domain case, but, in the multi-domain case that includes Schwarz iterations, Newton's method becomes first order. There is a loss of accuracy with the number of subdomains that can be related with some lack of regularity at the interfaces for Schwarz.

In relation to turbulence, the model can be near turbulence for the convenient values of  $R$ , but it cannot be turbulent because it is stationary. In Ref. [29], the authors consider the maximum value  $R = 10^5$  and plumes are observed in the experiments, but the flow is not yet turbulent. In other references, such as [71], a power-law relation between the Reynolds number and the Rayleigh number,  $Re = R^{1/2}$ , was found. A flow starts to be turbulent at approximately  $Re = 2000$ , following this power law; in our case, it corresponds to  $R = 4 \times 10^6$ , higher than our highest value  $R = 10^5$ . Turbulence can be modeled with direct numerical simulation (DNS), which would be our model including time dependency. As we do not include the time dependency in this work, we only look for stationary solutions. Now, the highest value of  $R$  is  $10^5$  which is not yet turbulent. The time dependent model for turbulence can be easily implemented, and it will be addressed in future work. Because of this domain decomposition, the aspect ratio and the Rayleigh number can be increased considerably by adding subdomains in any direction. Then, values of the Rayleigh number for near turbulent regimes can be reached, and domains with large aspect ratio can be considered. Namely, the great advantage of this method is that we get solutions close to turbulence, or in domains with large aspect ratios, by solving systems of linear equations with well-conditioned matrices of maximum size one thousand. The main benefit of the developed method compared with finite differences, finite elements, spectral elements, continuous Galerkin, and discontinuous Galerkin is the small well-conditioned matrices that appear in this method. The maximum size of the matrix in the systems that are solved with this method is  $10^3$  in the case of a mesh grid  $16 \times 12$  for a near turbulent flow with  $R = 10^5$ . This is the main advantage over other methods that require solving systems with huge matrices of the order of several million, usually badly conditioned. In this case, ill conditioning is avoided and there is no need for preconditioners; even domain decomposition is used as preconditioner for those methods, as, for example, in Refs. [55,72].

Regarding the computational cost, the size of the collocation mesh is around 100 points, the problem has four unknowns, then the size of the matrices is  $400 \times 400$ ; the linear solver needs this size squared operations, i.e.,  $O(10^5)$ , the Schwarz and Newton iterations are fixed to 5 and 40, respectively. Then, the computational cost is around the number of subdomains times  $10^7$ . The computational cost is comparable to other methods. The method is parallelizable; the number of subdomains can be eliminated from the count in this case, but then the computational cost penalty due to parallelization should be included.

## 5. Conclusions

In this work, an alternating Schwarz domain decomposition method to solve a Rayleigh–Bénard problem is presented. The problem is modeled with the stationary version of incompressible Navier–Stokes equations and the heat equation in a rectangular domain under the Boussinesq approximation. The system of partial differential equations is nonlinear. The nonlinearity has been solved numerically with a Newton's method. Each iteration of Newton's method has been discretized with an alternating Schwarz scheme, and each Schwarz iteration is solved with a collocation Legendre method. The Legendre collocation method is ill conditioned; for this reason it is not possible in a single domain to increase the mesh size appropriately to obtain solutions with many oscillations or solutions

with structure at different scales. These solutions appear for large domains or large values of the Rayleigh number in the turbulent regime. This difficulty has been overcome with the use of an alternating Schwarz domain decomposition method. The original domain has been divided into several subdomains in both directions of the plane. Each step of the Newton and Schwarz iteration problems in each subdomain has been solved by Legendre collocation with a coarse mesh, then the problem in each subdomain is well conditioned. The present work achieves an efficient alternating Schwarz algorithm such that the number of subdomains can be increased indefinitely in both directions of the plane. The method has been validated with a benchmark with numerical solutions obtained with other methods and with real experiments. Because of this domain decomposition method, the aspect ratio and Rayleigh number can be increased considerably by adding subdomains. Then Rayleigh values close to the turbulent regime can be reached. The great advantage of this method is that we obtain solutions close to turbulence, or in domains with large aspect ratios, by solving systems of linear equations with well-conditioned matrices of maximum size one thousand. This is an advantage over other methods that require solving systems with huge matrices on the order of several million, usually with conditioning problems. The computational cost is comparable to other methods, and the code is parallelizable.

**Author Contributions:** Investigation, D.M., H.H. and F.P.; Software, D.M., H.H. and F.P. All authors have read and agreed to the published version of the manuscript.

**Funding:** This work was partially supported by Research Grants PID2019-109652GB-I00 (Spanish Government) and 2021-GRIN-30985 (Universidad de Castilla-La Mancha), which include RDEF funds. D. Martínez has a predoctoral contract from the Universidad de Castilla-La Mancha, which includes ESF+ funds.

**Data Availability Statement:** Not applicable.

**Conflicts of Interest:** The authors declare no conflict of interest.

## References

1. Boffetta, G.; Ecke, R. Two-Dimensional Turbulence. *Annu. Rev. Fluid Mech.* **2012**, *44*, 427–451. [[CrossRef](#)]
2. Grinberg, L.; Karniadakis, G. A new domain decomposition method with overlapping patches for ultra-scale simulations: Application to biological flows. *J. Comput. Phys.* **2010**, *229*, 5541–5563. [[CrossRef](#)]
3. Herrero, H.; Pla, F.; Ruiz-Ferrández, M. A Schwarz Method for a Rayleigh-Bénard Problem. *J. Sci. Comput.* **2019**, *78*, 376–392. [[CrossRef](#)]
4. Keyes, D.E. Multiphysics simulations: Challenges and opportunities. *Int. J. High Perform. Comput. Appl.* **2012**, *27*, 4–86. [[CrossRef](#)]
5. Kim, J.W.; Sandberg, R.D. Efficient parallel computing with a compact finite difference scheme. *Comput. Fluids* **2012**, *58*, 70–87. [[CrossRef](#)]
6. Klinteberg, L.; Askham, T.; Kropinski, M.C. A fast integral equation method for the two-dimensional Navier-Stokes equations. *J. Comput. Phys.* **2020**, *409*, 109353. [[CrossRef](#)]
7. Manna, M.; Benocci, C.; Simons, E. Large eddy simulation of turbulent flows via domain decomposition techniques. Part 1: Theory. *Int. J. Numer. Methods Fluids* **2005**, *48*, 367–395. [[CrossRef](#)]
8. Mittal, K.; Dutta, S.; Fischer, P. Multirate timestepping for the incompressible Navier-Stokes equations in overlapping grids. *J. Comput. Phys.* **2021**, *437*, 110335. [[CrossRef](#)]
9. Utyuzhnikov, S. Domain decomposition for near-wall turbulent flows. *Comput. Fluids* **2009**, *38*, 1710–1717. [[CrossRef](#)]
10. Bénard, H. Les tourbillons cellulaires dans une nappe liquide. *Rev. Gen. Sci. Pures Appl.* **1900**, *11*, 1261–1271.
11. Rayleigh, L. On the convective currents in a horizontal layer of fluid when the temperature is on the under side. *Lond. Edinburg Dublin Philos. Mag. J. Sci.* **1916**, *32*, 529–546. [[CrossRef](#)]
12. Pearson, J.R.A. On convection cells induced by surface tension. *J. Fluid Mech.* **1958**, *4*, 489–500. [[CrossRef](#)]
13. Kolesnikov, A.I.; Grechishkin, R.M.; Tret'yakov, A.A.; Gritsunova, O.V.; Vorontsova, E.Y. Taylor Vortices Formed in the Melt during Paratellurite Crystal Growth. *Crystallogr. Rep.* **2014**, *53*, 1203–1207. [[CrossRef](#)]
14. Smirnov, Y.M.; Kaplunov, I.A.; Kolesnikov, A.I. Symmetry in the Crystal Growth Processes from the Melt. *Acta Crystallogr. A Found. Adv.* **2006**, *62*, S57. [[CrossRef](#)]
15. Hennenberg, M.; Weysson, B.; Slavtchev, S.; Alexandrov, V.; Desai, T.J. Rayleigh-Marangoni-Bénard instability of a ferrofluid layer in a vertical magnetic field. *J. Magn. Magn. Mater.* **2005**, *289*, 268–271. [[CrossRef](#)]
16. Buffone, C.; Cecere, A.; Savino, R.; Rioboo, R.; De Conick, J.; Vaerenberg, S. Onset of Marangoni convection in low viscosity silicon oil inside a heated capillary tube. *Int. J. Therm. Sci.* **2014**, *84*, 158–163. [[CrossRef](#)]

17. Hoyas, S.; Herrero, H.; Mancho, A.M. Thermocapillar and thermogravitatory waves in a convection problem. *Theor. Comput. Fluid Dyn.* **2004**, *18*, 309–322. [[CrossRef](#)]
18. Normand, C.; Pomeau, Y.; Velarde, M.G. Convective instability: A physicist's approach. *Rev. Mod. Phys.* **1977**, *49*, 581–624. [[CrossRef](#)]
19. Schatz, M.F.; Neitzel, G.P. Experiments on thermocapillary instabilities. *Annu. Rev. Fluid Mech.* **2001**, *33*, 93–127. [[CrossRef](#)]
20. Velarde, M.G.; Normand, C. Convection. *Sci. Am.* **1980**, *243*, 92–108.
21. Velarde, M.G.; Nepomnyashchy, A.A.; Hennenberg, M. Onset of oscillatory interfacial instabilities and wave motions in Benard layers. *Adv. Appl. Mech.* **2001**, *37*, 167–238. [[CrossRef](#)]
22. Colinet, P.; Legros, J.C.; Velarde, M.G. *Nonlinear Dynamics of Surface Tension-Driven Instabilities*; Wiley-VCH: New York, NY, USA, 2001.
23. Chandrasekhar, S. *Hydrodynamic and Hydromagnetic Stability*; Dover: New York, NY, USA, 1981.
24. Khallouf, H.; Gershuni, G.Z.; Mojtabi, A. Numerical study of 2-dimensional thermovibrational convection in rectangular cavities. *Numer. Heat Transf. Part A Appl.* **1995**, *27*, 297–305. [[CrossRef](#)]
25. Koschmieder, E.L. *Bénard Cells and Taylor Vortices*; Cambridge University Press: Cambridge, UK, 1993.
26. Pla, F.; Herrero, H.; Lafitte, O. Theoretical and numerical study of a thermal convection problem with temperature-dependent viscosity in an infinite layer. *Physica D* **2010**, *239*, 1108–1119. [[CrossRef](#)]
27. Platten, J.K.; Legros, J.C. Dynamics of the Rayleigh-Bénard convection. *J. Non-Equilib. Thermodyn.* **1980**, *5*, 243–254. [[CrossRef](#)]
28. Peyret, R. *Spectral Methods for Incompressible Viscous Flow*; Applied Mathematical Sciences 148; Springer: Berlin/Heidelberg, Germany, 2002.
29. Lithgow-Bertollini, C.; Richards, M.A.; Conrad, C.P.; Griffiths, R.W. Plume generation in natural thermal convection at high Rayleigh and Prandtl numbers. *J. Fluid Mech.* **2001**, *434*, 1–21. [[CrossRef](#)]
30. Pandey, A.; Verma, M.K.; Chatterjee, A.G.; Dutta, B. Similarities between 2D and 3D convection for large Prandtl number. *Pramana* **2016**, *87*, 1–10. [[CrossRef](#)]
31. Bernardi, C.; Maday, Y. *Approximations Spectrales des Problemes aux Limites Elliptiques*; Springer: Berlin, Germany, 1992.
32. Canuto, C.; Hussaini, M.; Quarteroni, A.; Zang, T. *Spectral Methods in Fluid Dynamics*; Springer: New York, NY, USA, 1988.
33. Castaño, D.; Navarro, M.C.; Herrero, H. Thermoconvective vortices in a cylindrical annulus with varying inner radius. *Chaos* **2014**, *24*, 043116. [[CrossRef](#)]
34. Herrero, H.; Mancho, A.M. Influence of aspect ratio in convection due to nonuniform heating. *Phys. Rev. E* **1998**, *57*, 7336–7339. [[CrossRef](#)]
35. Cai, X.-C. *Some Domain Decomposition Algorithms for Nonselfadjoint Elliptic and Parabolic Partial Differential Equations*; Palala Press: Online, 2018.
36. Mathew, T.P.A. *Domain Decomposition Methods for the Numerical Solution of Partial Differential Equations*; Springer: Berlin/Heidelberg, Germany, 2008.
37. Quarteroni, A.; Valli, A. *Domain Decomposition Methods for Partial Differential Equations*; Oxford Science Publications: Oxford, UK, 1999.
38. Smith, B.; Bjorstad, P.; Gropp, W. *Domain Decomposition: Parallel Multilevel Methods for Elliptic Partial Differential Equations*; Cambridge University Press: Cambridge, UK, 1996.
39. Toselli, A.; Widlund, O. *Domain Decomposition Methods- Algorithms and Theory*; Springer: Berlin/Heidelberg, Germany, 2010.
40. Wildlund, O.B.; Keyes, D.E. *Domain Decomposition Methods in Science and Engineering XVI*; Springer: Berlin/Heidelberg, Germany, 2007.
41. Blayo, E.; Cherel, D.; Rousseau, A. Towards optimized Schwarz methods for the Navier-Stokes equations. *J. Sci. Comput.* **2016**, *66*, 275–295. [[CrossRef](#)]
42. Brakkee, E.; Vuik, C.; Wesseling, P. Domain decomposition for the incompressible Navier-Stokes equations: Solving subdomains accurately and inaccurately. *Int. J. Numer. Methods Fluids* **1998**, *26*, 1217–1237. [[CrossRef](#)]
43. Mittal, K.; Dutta, S.; Fischer, P. Nonconforming Schwarz-spectral element methods for incompressible flow. *Comput. Fluids* **2019**, *191*, 104237. [[CrossRef](#)]
44. Muller, L.; Lube, G. A nonoverlap domain decomposition method for the nonstationary Navier-Stokes problem. *ZAMM J. Appl. Math. Mech.* **2001**, *81*, 725–726. [[CrossRef](#)]
45. Ronquist, E.M. A domain decomposition solver for the steady Navier-Stokes equations. In Proceedings of the Third International Conference on Spectral and High Order Methods, Houston, TX, USA, 5–9 June 1995; pp. 469–485.
46. Shang, Y. A parallel finite element variational multiscale method based on fully overlapping domain decomposition for incompressible flows. *Numer. Methods Partial. Differ. Equ.* **2015**, *31*, 856–875. [[CrossRef](#)]
47. Strikwerda, J.; Scarnick, C. A domain decomposition method for incompressible flow. *SIAM J. Sci. Comput.* **1993**, *14*, 49–67. [[CrossRef](#)]
48. Tang, H.S.; Haynes, R.D.; Houzeaux, G. A Review of Domain Decomposition Methods for Simulation of Fluid Flows: Concepts, Algorithms, and Applications. *Arch. Comput. Meth. Eng.* **2021**, *28*, 841–873. [[CrossRef](#)]
49. Xu, X.; Chow, C.; Lui, S. On nonoverlapping domain decomposition methods for the incompressible Navier-Stokes equations. *ESAIM Math. Model. Numer. Anal.* **2005**, *39*, 1251–1269. [[CrossRef](#)]

50. Louchart, O.; Randriamampianina, A. A spectral iterative domain decomposition technique for the incompressible Navier-Stokes equations. *Appl. Numer. Math.* **2000**, *33*, 233–240. [[CrossRef](#)]
51. Cai, X.C.; Keyes, D.E. Nonlinearly preconditioned inexact Newton algorithms. *SIAM J. Comput. Sci.* **2002**, *24*, 183–200. [[CrossRef](#)]
52. Chien, H.; Mark, C.; Tchelepi, H.A.; Yardumian, H.E.; Chen, W.H. Scalable parallel multi-purpose reservoir simulator. *SPE Symp. Reserv. Simul.* **1997**, 17–30. [[CrossRef](#)]
53. Lacroix, S.; Vassilevski, Y.; Wheeler, J.; Wheeler, M.F. Iterative solution methods for modeling multiphase flow in porous media fully implicitly. *SIAM J. Sci. Comput.* **2003**, *25*, 905–926. [[CrossRef](#)]
54. Barnafi, N.A.; Pavarino, L.F.; Scacchi, S. Parallel inexact Newton-Krylov and quasi-Newton solvers for nonlinear elasticity. *arXiv* **2022**, arXiv:2203.05610.
55. Klemetsdal, O.; Moncorgé, A.; Moyner, O.; Lie, K.A. A numerical study of the additive Schwarz preconditioned exact Newton method (ASPEN) as a nonlinear preconditioner for immiscible and compositional porous media flow. *Comput. Geosci.* **2022**, *26*, 1045–1063. [[CrossRef](#)]
56. Wu, Y.; Liu, B.; Zang, H.; Li, F. Accuracy and efficient solution of helical coiled once-through steam generator model using JFNK method. *Ann. Nucl. Energy* **2021**, *159*, 108290. [[CrossRef](#)]
57. Klemetsdal, O.S.; Moyner, O.; Lie, K.-A. Robust nonlinear Newton solver with adaptive interface-localized trust regions. *SPE J.* **2019**, *24*, 1576–1594. [[CrossRef](#)]
58. Moyner, O. Nonlinear solver for three-phase transport problems based on approximate trust regions. *Comput. Geosci.* **2017**, *21*, 999–1021. [[CrossRef](#)]
59. Cortés, J.; Herrero, H.; Pla, F. A Galerkin/POD Reduced-Order Model from Eigenfunctions of Non-Converged Time Evolution Solutions in a Convection Problem. *Mathematics* **2022**, *10*, 905. [[CrossRef](#)]
60. Herrero, H.; Maday, Y.; Pla, F. RB (Reduced Basis) applied to RB (Rayleigh-Bénard). *Comput. Methods Appl. Mech. Eng.* **2013**, *261–262*, 132–141. [[CrossRef](#)]
61. Mercader, I.; Batiste, O.; Alonso, A. Continuation of travelling-wave solutions of the Navier-Stokes equations. *Int. J. Numer. Methods Fluids* **2006**, *52*, 707–721. [[CrossRef](#)]
62. Navarro, M.C.; Castaño, D.; Herrero, H. Thermoconvective instabilities to explain the main characteristics of a dust devil-like vortex. *Physica D* **2015**, *308*, 109–115. [[CrossRef](#)]
63. Pla, F.; Mancho, A.M.; Herrero, H. Bifurcation phenomena in a convection problem with temperature dependent viscosity at low aspect ratio. *Physica D* **2009**, *238*, 572–580. [[CrossRef](#)]
64. Bustamante, C.A.; Power, H.; Florez, W.F. Schwarz alternating domain decomposition approach for the solution of mixed heat convection flow problems based on the method of approximate particular solutions. In *Computational Methods for Coupled Problems in Science and Engineering V*; Idelsohn, S., Papadrakakis, M., Schrefler, B., Eds.; UPCCommons: Barcelona, Spain, 2013; pp. 1280–1291.
65. Davies, G.F. *Dynamic Earth. Plates, Plumes and Mantle Convection*; Cambridge University Press: Cambridge, UK, 1999.
66. Moresi, L.N.; Solomatov, V.S. Numerical investigation of 2D convection with extremely large viscosity variations. *Phys. Fluids* **1995**, *7*, 2154–2162. [[CrossRef](#)]
67. Herrero, H.; Mancho, A.M. On pressure boundary conditions for thermoconvective problems. *Int. J. Numer. Methods Fluids* **2002**, *39*, 391–402. [[CrossRef](#)]
68. Herrero, H.; Hoyas, S.; Donoso, A.; Mancho, A.M.; Chacón, J.M.; Portugués, R.F.; Yeste, B. Chebyshev collocation for a convective problem in primitive variable formulation. *J. Sci. Comput.* **2003**, *8*, 312–328.
69. Ghias, S.R.; Jarvis, G.T. Mantle convection models with temperature and depth-dependent thermal expansivity. *J. Geophys. Res. Solid Earth* **2008**, *113*, 1–15. [[CrossRef](#)]
70. Mancho, A.M.; Herrero, H.; Burguete, J. Primary instabilities in convective cells due to non-uniform heating. *Phys. Rev. E* **1997**, *56*, 2916–2923. [[CrossRef](#)]
71. Mazzino, A. Two-dimensional turbulence. *Phys. Fluids* **2017**, *29*, 111102. [[CrossRef](#)]
72. Wu, B.T.; Wang, Z.D.; Wang, H.M. A GPU-Based Multilevel Additive Schwarz Preconditioner for Cloth and Deformable Body Simulation. *AC Trans. Graph.* **2022**, *41*, 1–14. [[CrossRef](#)]